Available online at www.sciencedirect.com
SCIENCE DIRECT
ELSEVIER
International Journal of Solids and Structures 43 (2006) 5811–5835
INTERNATIONAL JOURNAL OF SOLIDS and STRUCTURES
www.elsevier.com/locate/ijsolstr

Propagation of a plane-strain hydraulic fracture with a fluid lag: Early-time solution

Dmitry I. Garagash *

Clarkson University, Department of Civil and Environmental Engineering, 8 Clarkson Ave., Potsdam, NY 13699-5710, USA

Received 12 May 2005
Available online 20 December 2005

Abstract

This paper studies the propagation of a plane-strain fluid-driven fracture with a fluid lag in an elastic solid. The fracture is driven by a constant rate of injection of an incompressible viscous fluid at the fracture inlet. The leak-off of the fracturing fluid into the host solid is considered negligible. The viscous fluid flow is lagging behind an advancing fracture tip, and the resulting tip cavity is assumed to be filled at some specified low pressure with either fluid vapor (impermeable host solid) or pore-fluids infiltrating from the permeable host solid. The scaling analysis allows to reduce problem parametric space to two lumped dimensionless parameters with the meaning of the solid toughness and of the tip underpressure (difference between the specified pressure in the tip cavity and the far field confining stress). A constant lumped toughness parameter uniquely defines solution trajectory in the parametric space, while time-varying lumped tip underpressure parameter describes evolution along the trajectory. Further analysis identifies the early and large time asymptotic states of the fracture evolution as corresponding to the small and large tip underpressure solutions, respectively. The former solution is obtained numerically herein and is characterized by a maximum fluid lag (as a fraction of the crack length), while the latter corresponds to the zero-lag solution of Spence and Sharp [Spence, D.A., Sharp, P.W., 1985. Self-similar solution for elastohydrodynamic cavity flow. Proc. Roy. Soc. London, Ser. A (400), 289–313]. The self-similarity at small/large tip underpressure implies that the solution for crack length, crack opening and net fluid pressure in the fluid-filled part of the crack is a given power-law of time, while the fluid lag is a constant fraction of the increasing fracture length. Evolution of a fluid-driven fracture between the two limit states corresponds to gradual expansion of the fluid-filled region and disappearance of the fluid lag. For small solid toughness and small tip underpressure, the fracture is practically devoid of fluid, which is localized into a narrow region near the fracture inlet. Corresponding asymptotic solution on the fracture lengthscale corresponds to that of a crack loaded by a pair of point forces which magnitude is determined from the coupled hydromechanical solution in the fluid-filled region near the crack inlet. For large solid toughness, the fluid lag is vanishingly small at any underpressure and the solution is adequately approximated by the zero-lag self-similar large toughness solution at any stage of fracture evolution. The small underpressure asymptotic solutions obtained in this work are sought to provide initial condition for the propagation of fractures which are initially under plane-strain conditions.

Keywords: Hydraulic fracture; Fluid lag; Confining stress; Asymptotic solutions

* Tel.: +1 315 268 6501; fax: +1 315 268 7985.
E-mail address: garagash@clarkson.edu

0020-7683/$ - see front matter
doi:10.1016/j.ijsolstr.2005.10.009

1. Introduction

Problem of a fluid-driven fracture arises in a variety of applications including stimulation of hydrocarbon reservoirs (Economides and Nolte, 2000), sequestration of CO_2 (Rudnicki, 2000), compensation grouting (Au, 2001), environmental subsurface remediation (Murdoch, 2002), induced caving in mining (Jeffrey and Mills, 2000) and transport of magma in the Earth's crust (Spence and Turcotte, 1985). Corresponding models of such fractures may vary in the level of complexity and detailing of physical processes involved. A basic model would include adequate description of the flow of a viscous pressurized fluid in the fracture channel, of the mechanical response of the fractured solid medium due to the loading by the pressurized fluid along the fracture channel walls and by the far field stresses, and of the conditions for fracture propagation in brittle solid. The rigorous mathematical solutions of these models, however, have proven to be very difficult even under simplifying assumption of planar or radial fracture geometries. This state of affairs lies with at least the following two generic issues: (i) inherent coupling of non-linear fluid flow in the fracture channel with the non-local mechanical response of the fracture (shape and extent), and (ii) the presence of a priori unknown fluid lag adjacent to the fracture leading edge.

The lagging of the fracturing fluid front behind the front of advancing fracture, a subject of discussion in the modeling community since the seminal contribution of Khristianovic and Zheltov (1955), has been directly observed in experiments in the low confining stress environment (Medlin and Masse, 1984; Groenenboom et al., 2001; Bunger et al., 2005). However, in the view of the complicated nature of the problem, most of the analytical efforts resulted in either solutions of a zero-lag fracture treating the hydromechanical coupling to a various degree of rigor (e.g., Perkins and Kern, 1961; Geertsma and de Klerk, 1969; Abé et al., 1976; Spence and Sharp, 1985; Huang et al., 1990; Carbonell et al., 1999; Savitski and Detournay, 2002; Garagash, in press; Garagash and Detournay, 2005) or in solutions of a fracture with a priori unknown lag under various assumptions relaxing the hydromechanical coupling, e.g., assumption of a uniform fluid pressure in the fracture (Khristianovic and Zheltov, 1955; Barenblatt, 1956; Jeffrey, 1989; Advani et al., 1997; Bui, 1996). Apart from the above contributions, Nilson (1981) has considered hydromechanically coupled similarity solutions for an edge fracture in a zero-toughness solid driven by a compressible gas under a constant pressure boundary condition at the inlet. These solutions, characterized by an exponentially fast fracture growth, have shown a profound influence of the lag which can account for 15–75% of the fracture length when the gas pressure at the inlet is 2–10 times the remote confining stress.

The strong non-linear hydromechanical coupling in the vicinity of the fracture front yields very high fluid pressure gradients, which yield a negative singularity of the fluid pressure when the fluid is assumed to reach the fracture front, as in the zero-lag approximation. In particular, if the mechanical response is governed by the Linear Elastic Fracture Mechanics (LEFM) and the flow of a Newtonian fluid in the fracture is governed by the unidirectional lubrication theory, the fluid pressure behaves as $p_f \sim \ln \hat{x}$ in the finite fracture toughness case and as $p_f \sim -\hat{x}^{-1/3}$ in the zero toughness case, where $\hat{x}$ is the normal distance to the fracture edge (Spence and Sharp, 1985; Lister, 1990; Desroches et al., 1994). Since a fluid cannot sustain infinite suction, a cavity devoid of the fracturing fluid has to be naturally present near the fracture advancing edge. In the case of an impermeable medium, this cavity is filled with the vapors of the fracturing fluid under approximately constant vapor pressure. Alternatively, in the case of a permeable saturated medium, the cavity is filled with the pore fluid which is continuously sucked into the fracture at its advancing edge and is expelled back into the medium near the fracturing fluid/pore fluid interface (Rubin, 1993; Detournay and Garagash, 2003). The physical role of a fluid lag in the formulation of a fluid-driven fracture is analogous to that of a "process zone" in fracture mechanics: the former allows for the finiteness of the fluid pressure immediately behind the fracture front and the latter allows for the finiteness of the stresses immediately ahead of the front.

As often in the treatment of the process zone in the traditional fracture mechanics, the fluid lag is often assumed to be small compared to the fracture extent and irrelevant in fracture propagation. The details of the coupled hydromechanical solution in the vicinity of the fracture edge when a fluid lag is small compared to the fracture lengthscale has been previously studied in the approximation of a semi-infinite steadily advancing fracture (Lister, 1990; Garagash and Detournay, 2000; Detournay and Garagash, 2003). Herein, we present a general fully-coupled hydromechanical analysis of a fluid-driven fracture with a fluid lag which is not a priori small on the fracture lengthscale. This analysis is applied to a finite fracture with the plane-strain

geometry (Griffith's crack) driven by a fluid injected at a constant rate at the crack inlet. The analysis bears the essential methodology which can be used to evaluate the lag behavior in other finite fracture geometries (e.g., radial fracture). Furthermore, this analysis allows to delineate in the space of problem parameters the fracture propagation regimes where the lag is appreciable fraction of the fracture length and, therefore, has a direct influence on the fracture propagation, and the regimes where the zero-lag assumption is appropriate.

The paper is organized as follows. The model of a plane-strain fluid-driven fracture with a lag is presented in Section 2 followed by the scaling considerations in Section 3. The problem scaling identifies a pair of dimensionless lumped parameters with the meaning of the tip underpressure (the difference between the pressure in the lag region and the far field confining stress) and of the effective toughness or viscosity, respectively, which fully define a unique solution. Fracture propagation regimes corresponding to the limiting states of fracture evolution are then anticipated and further related to the evolution of the fluid lag at a constant value of the lumped toughness parameter. Fracture evolution takes place between the self-similar zero tip underpressure solution and the self-similar infinite tip underpressure solution; and is accompanied by evolving (decreasing) fluid lag, as a fraction of fracture length: from a maximum toughness-dependent value to zero, respectively. Section 4 describes related asymptotic solutions in the following order: (i) the small tip underpressure, small toughness solution; (ii) arbitrary tip underpressure, large toughness solution; and (iii) zero tip underpressure, arbitrary toughness solution. Discussion of these solutions and their possible physical significance on the basis of scaling analysis for shallow hydraulic fractures and magma-driven fractures in the upper crust is given in Section 5. Section 6 follows with some conclusions.

2. Problem formulation

Consider a usual model of a plane-strain fluid-driven fracture with zero lag (e.g., Spence and Sharp, 1985) extended to account for a non-zero fluid lag. A two-dimensional hydraulic fracture of half length $\ell(t)$ is propagating in an infinite linear elastic medium characterized by the Young modulus E, Poisson ratio ν, and toughness K_{Ic} (Fig. 1). An incompressible Newtonian fluid with viscosity μ is injected at the center of the fracture at a constant volumetric rate Q_o (per unit fracture out-of-plane width) to drive the fracture. The leak-off of the fracturing fluid into the solid is considered negligible. The fracture is loaded by the internal fluid pressure $p_{\mathrm{f}}(x, t)$ and by the far-field confining stress σ_o perpendicular to the fracture plane. Fluid front $x = \ell_{\mathrm{f}}(t)$ is allowed to lag behind the fracture front $x = \ell(t)$. A lag region of a priori unknown length $\ell - \ell_{\mathrm{f}}$ adjacent to a fracture tip is assumed to be filled at a specified constant pressure $p_{\mathrm{f(tip)}}$ by either the evaporated fracturing fluid (in the case of impermeable host solid) or by the pore-fluid infiltrated from the permeable host solid. The surface tension effects (Bui, 1996) are neglected so that the pressure is continuous at the fluid front.

The solution of the fluid-driven fracture problem is given by the net fluid pressure $p(x, t) = p_{\mathrm{f}}(x, t) - \sigma_o$, the fracture opening $w(x, t)$, the fracture half-length $\ell(t)$, and the half-length of the 'fluid channel'[1] $\ell_{\mathrm{f}}(t)$ as a function of the position x along the fracture (p and w only), time t, and five problem parameters. These parameters are injection rate Q_o, the *tip underpressure*

$$-p_{\mathrm{t}} = \sigma_o - p_{\mathrm{f(tip)}} \tag{1}$$

and the three material parameters (multiplied by numerical factors with a purpose to tidy up the governing equations)

$$\mu' = 12\mu, \quad E' = \frac{E}{1-\nu^2}, \quad K' = 4\left(\frac{2}{\pi}\right)^{1/2} K_{\mathrm{Ic}} \tag{2}$$

with the meaning of fluid viscosity, solid elastic modulus, and solid toughness, respectively.

For an impermeable solid and high confining stress σ_o (e.g., fractures in the crust at depth), $p_{\mathrm{f(tip)}}$, which has the meaning of the equilibrium vapor pressure, is usually negligible compared to σ_o. As the result, the tip underpressure can be approximated by the confining stress, $(-p_{\mathrm{t}}) \simeq \sigma_o$. For permeable solids, the tip cavity is filled by the pore fluid sucked into the fracture at an advancing fracture tip, and, $p_{\mathrm{f(tip)}}$, in general, has a

[1] Fluid-filled part of the crack.

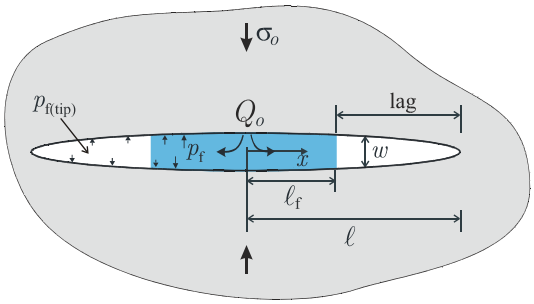

Fig. 1. Sketch of a two-dimensional fluid-driven fracture.

non-uniform distribution along the tip cavity (Detournay and Garagash, 2003), with the exception for the following two limiting cases. The first limiting case corresponds to fast fracture propagation (or nearly impermeable solid) when significant depression of pore fluid pressure at the fracture front causes cavitation of the pore fluid in the tip cavity, and $p_{f(tip)}$ is given by the pore-fluid vapor pressure. The second limiting case corresponds to slow fracture propagation (or very permeable solid) when pore fluid pressure in the lag is uniform and equilibrated with the far field pore pressure p_o, and the tip underpressure is equal to the far-field effective confining stress, $(-p_t) = \sigma_o - p_o$.

The analysis presented herein makes use of the assumption of a *constant underpressure* in the lag region, and, therefore, is strictly applicable to either the case of impermeable solid or the two limiting cases of permeable solid as outlined above. Additionally, the analysis assumes that tip underpressure is non-negative, $(-p_t) \geqslant 0$, or equivalently, that the net-loading in the lag region is compressive,[2] $p_t \leqslant 0$, and it acts to inhibit fracture propagation.

Using problem symmetry with respect to the crack inlet $x = 0$, governing equations and boundary conditions are presented over the half of the crack, $0 \leqslant x \leqslant \ell$, as follows.

Fluid flow in the fracture. Fluid flow in the fluid-filled part of the fracture is described by equations of lubrication theory (Batchelor, 1967), namely, local and global continuity equations and the Poiseuille law. The integral form of the local continuity equation and the Poiseuille law can be written as

$$\frac{\partial}{\partial t}\int_x^{\ell_f} w\,dx = q, \quad q = -\frac{w^3}{\mu'}\frac{\partial p}{\partial x} \qquad (0 \leqslant x < \ell_f) \tag{3}$$

where q is the fluid flow rate per unit (out-of-plane) width. Global fluid continuity requires the injected fluid volume per unit crack out-of-plane width to be equal to the volume of the fluid-filled part of the fracture,

$$2\int_0^{\ell_f} w\,dx = Q_o t \tag{4}$$

In the fluid lag zone,

$$p(x,t) = p_t < 0 \quad (\ell_f \leqslant x \leqslant \ell) \tag{5}$$

According to the fluid (and net) pressure continuity, lag condition (5) provides the net-pressure boundary condition at the fluid front $x = \ell_f$ for the fluid flow equations (3).

Fracture opening. Net-pressure p is related to the dislocation density $\partial w/\partial x$ by an integral relation of the linear elasticity theory (e.g., Bilby and Eshelby, 1968)

$$p(x,t) = -\frac{E'}{2\pi}\int_0^{\ell}\frac{\partial w(s,t)}{\partial s}\frac{s\,ds}{s^2 - x^2} \quad (0 \leqslant x \leqslant \ell) \tag{6}$$

Sneddon and Lowengrub (1969) provide an inverse of Eq. (6), which, on account of Eq. (5), has the form

[2] The far field confining stress $\sigma_o \geqslant p_{f(lag)} \geqslant 0$.

$$w(x,t) = \int_0^{\ell_f} G\left(\frac{x}{\ell},\frac{s}{\ell}\right)\frac{p(s,t)}{E'}\,\mathrm{d}s + \frac{p_t}{E'}\int_{\ell_f}^{\ell} G\left(\frac{x}{\ell},\frac{s}{\ell}\right)\mathrm{d}s \quad (0 \leqslant x \leqslant \ell) \tag{7}$$

The integral kernel G is defined by

$$G(\xi,\xi') = \frac{4}{\pi}\ln\left|\frac{(1-\xi^2)^{1/2}+(1-\xi'^2)^{1/2}}{(1-\xi^2)^{1/2}-(1-\xi'^2)^{1/2}}\right| \tag{8}$$

Fracture propagation. The LEFM fracture propagation criterion (e.g., Kanninen and Popelar, 1985) relies on the assumption of mobile equilibrium, whereby the mode I fracture stress intensity factor K_I is equal to the solid toughness K_{Ic},

$$K_I = K_{Ic} \tag{9}$$

The propagation condition (9) can be expressed as an asymptotic condition for the fracture opening at the tip (Irvin, 1957)

$$w = \frac{K'}{E'}(\ell - x)^{1/2} \quad (\ell - x \ll \ell) \tag{10}$$

The equivalent form of Eq. (9) is obtained from the expression for K_I for a plane-strain crack in the form which makes use of the uniform net loading in the lag, Eq. (5),

$$K' = \frac{8}{\pi}(2\ell)^{1/2}\left(\int_0^{\ell_f}\frac{p(x,t)\,\mathrm{d}x}{\left(\ell^2-x^2\right)^{1/2}} + p_t\int_{\ell_f}^{\ell}\frac{\mathrm{d}x}{(\ell^2-x^2)^{1/2}}\right) \tag{11}$$

3. Scaling

Let us consider normalized fracture length γ, normalized fluid channel length γ_f, normalized net-pressure Π and normalized fracture opening Ω in the form inspired by the scaling analysis of the zero-lag fracture (Detournay, 2004)

$$\begin{aligned} \ell(t) &= L(t)\gamma(t) \\ \ell_f(t) &= L(t)\gamma_f(t) \\ p(x,t) &= \varepsilon(t)E'\Pi(\xi,t) \\ w(x,t) &= \varepsilon(t)L(t)\Omega(\xi,t) \end{aligned} \tag{12}$$

where $L(t)$ is the lengthscale of the fluid channel and $\varepsilon(t)$ is a small factor $O(p/E')$. The normalized field variables introduced above are a function of time t and a spatial coordinate, which can be taken in either of the forms:

$$\xi = \frac{x}{\ell(t)}, \quad \zeta = \frac{x}{\ell_f(t)} \tag{13}$$

The 'crack coordinate' ξ is useful to formulate equations along the whole crack extent ($x \in (0, \ell)$ corresponds to $\xi \in (0, 1)$) such as elasticity equation (7), while the 'channel coordinate' ζ is useful to formulate equations along the channel (fluid-invaded) part of the crack ($x \in (0, \ell_f)$ corresponds to $\zeta \in (0, 1)$). The fluid front position in the ξ-coordinate is denoted by ξ_f and can be also interpreted as the 'fluid fraction' (i.e. the channel length as the fraction of the crack length):

$$\xi_f(t) = \frac{\ell_f(t)}{\ell(t)} = \frac{\gamma_f(t)}{\gamma(t)} \tag{14}$$

The normalized fluid lag (i.e., the lag length as the fraction of the crack length) is $1 - \xi_f$. The fluid fraction ξ_f can vary between asymptotic zero value ($\xi_f \to 0$) and the unity ($\xi_f = 1$) corresponding to the dry fracture (maximum lag) and to the fully fluid-filled fracture (zero lag), respectively.

The basis for the scaling, Eqs. (12), can be explored by considering elasticity equation (7) and the lag condition (5). Fracture opening w is comprised from positive contribution of $O(\ell_f p/E')$ from the loading in the fluid channel and negative contribution $O((\ell-\ell_f)p_t/E')$ from the loading in the lag. Since the former exceeds the absolute value of the latter for an open crack ($w \geqslant 0$), the opening scales with the loading in the fluid channel, $w = O(\ell_f p/E')$. Then scaling for the crack opening, Eq. $(12)_d$, follows from Eqs. $(12)_{b-c}$ if $L(t)$ has the meaning of the fluid channel lengthscale, $L = O(\ell_f)$. Accordingly, the normalized field variables introduced in Eqs. (12) are O(1) with possible exception for the normalized fracture length, $\gamma = O(\ell/\ell_f) = O(\xi_f^{-1})$, which can be large if the extent of the fluid channel, parametrized by ξ_f, is small.

Expression for the small parameter $\varepsilon(t)$ follows from the fluid global continuity (4), which suggests that $w\ell_f = O(Q_o t)$, and together with Eqs. $(12)_{b-d}$ yields

$$\varepsilon(t) = \frac{Q_o t}{L^2(t)} \tag{15}$$

A choice of the lengthscale $L(t)$, which, in view of Eq. (15), actually defines particular scaling, Eqs. (12), will be discussed following the introduction of the normalized equations.

3.1. Normalized equations in terms of the channel coordinate ζ

Substitution of the scaling equations (12) and of the convenient alternative form for the normalized fracture opening

$$\bar{\Omega}_f = \frac{\Omega}{\gamma_f} \tag{16}$$

into governing equations (3)–(11) results in the set of normalized equations expressed below in terms of the channel coordinate ζ. (Expression of the normalized equations in terms of the crack coordinate ξ ($=\xi_f\zeta$) is given in Appendix A.)

- Lubrication equation

$$\left[1 + 2\frac{t\dot{\gamma}_f}{\gamma_f}\right]\int_\zeta^1 \bar{\Omega}_f \,d\zeta + \left[\delta + \frac{t\dot{\gamma}_f}{\gamma_f}\right]\zeta\bar{\Omega}_f + \int_\zeta^1 t\dot{\bar{\Omega}}_f \,d\zeta = -\frac{\bar{\Omega}_f^3}{\mathscr{M}}\frac{\partial \Pi}{\partial \zeta}, \quad \zeta \in (0,1) \tag{17}$$

  where the superposed dot corresponds to the partial time derivative at fixed ζ, $(\partial/\partial t)_{|\zeta}$, and $\delta = t\dot{L}/L$ is equal to a constant 2/3 for fracture scalings defined in Section 3.2.
- Pressure condition in the lag

$$\Pi = -\mathscr{T}, \quad \zeta \in [1, \xi_f^{-1}] \tag{18}$$

- Global continuity

$$2\gamma_f^2 \int_0^1 \bar{\Omega}_f \,d\zeta = 1 \tag{19}$$

- Elasticity

$$\bar{\Omega}_f = \int_0^1 G_f(\zeta,\zeta')\Pi(\zeta',t)\,d\zeta' - \mathscr{T}\int_1^{1/\xi_f} G_f(\zeta,\zeta')\,d\zeta', \quad \zeta \in (0, \xi_f^{-1}) \tag{20}$$

  where scaled elastic kernel is $G_f(\zeta,\zeta') = G(\xi_f\zeta, \xi_f\zeta')$.
- Propagation condition

$$\bar{\Omega}_f = \frac{\mathscr{K}}{\xi_f^{1/2}}\gamma_f^{-1/2}(1-\xi_f\zeta)^{1/2}, \quad 1-\xi_f\zeta \ll 1 \tag{21}$$

  or, alternatively,

$$\frac{\mathscr{K}}{\xi_{\mathrm{f}}^{1/2}} = \frac{2^{7/2}}{\pi}\gamma_{\mathrm{f}}^{1/2}\left(\int_0^1 \frac{\Pi\,\mathrm{d}\zeta}{\left(1-\xi_{\mathrm{f}}^2\zeta^2\right)^{1/2}} - \frac{\mathscr{T}}{\xi_{\mathrm{f}}}\arccos\xi_{\mathrm{f}}\right) \tag{22}$$

Solution $\mathscr{F}(\zeta,t)=\{\Omega,\Pi,\gamma_{\mathrm{f}},\xi_{\mathrm{f}}\}$ of the above set of normalized equations (17)–(22) with (16) depends on the set of three dimensionless groups associated with viscosity, toughness, and tip underpressure, respectively,

$$\mathscr{M} = \frac{\mu'}{tE'\varepsilon^3}, \quad \mathscr{K} = \frac{K'}{\varepsilon E' L^{1/2}}, \quad \mathscr{T} = \frac{-p_{\mathrm{t}}}{\varepsilon E'} = \frac{\sigma_o - p_{\mathrm{f(tip)}}}{\varepsilon E'} \tag{23}$$

where ε is the function, Eq. (15), of the lengthscale L.

3.2. Viscosity and toughness scalings

To establish a particular scaling of the form given by Eqs. (12) and (15), the fluid channel lengthscale $L(t)$ has to be specified, for example, by setting one of the dimensionless groups, Eq. (23), to unity. The remaining two groups will constitute dimensionless parameters governing the normalized solution of Eqs. (17)–(22). Similarly to the zero-lag case (Detournay, 2004), by setting either $\mathscr{M}=1$ or $\mathscr{K}=1$ one can obtain the 'viscosity'- or 'toughness'-scaling characterized by the lengthscale L independent of the toughness K' or viscosity μ', respectively. The viscosity scaling can be physically motivated by a propagation regime where the effect of toughness K' is small compared to that of the fluid viscosity μ'. The toughness scaling can be motivated by a regime where the effect of viscosity is small compared to that of toughness. Argument about dominant energy dissipation mechanism (viscous dissipation in the fluid versus dissipation due to the fracturing of the solid) can be also used to delineate the above two regimes (Detournay, 1999). Analogously introduced 'tip underpressure'-scaling ($\mathscr{T}=1$) cannot be physically motivated, since the effect of the underpressure in the lag region is never a dominant one for an open propagating crack when compared to the effect of the net fluid loading on either the crack opening expression (20) or the crack propagation condition (22).

Expressions for the lengthscale L in the viscosity- and toughness-scalings and corresponding expressions for the dimensionless groups are listed in Table 1. The normalized solution $\mathscr{F}(\zeta,t)=\{\Omega,\Pi,\gamma_{\mathrm{f}},\xi_{\mathrm{f}}\}$ in the viscosity or toughness scalings is a function of the dimensionless position ζ, an evolutionary tip underpressure parameter ($\mathscr{T}_m(t)$ or $\mathscr{T}_k(t)$), and a constant parameter ($\mathscr{K}_m$ or $\mathscr{M}_k$): $\mathscr{F}=\mathscr{F}_m(\zeta,\mathscr{T}_m,\mathscr{K}_m)$ and $\mathscr{F}=\mathscr{F}_k(\zeta,\mathscr{T}_k,\mathscr{M}_k)$, respectively.

Substitution of the appropriate expressions for the dimensionless groups $\mathscr{M}$, $\mathscr{K}$, and $\mathscr{T}$ from Table 1 into Eqs. (17)–(22) yields two sets of governing equations in the viscosity and toughness scalings, respectively. The time derivative terms $t(\partial/\partial t)$ in lubrication equation (17) can be expressed in terms of the derivative in evolutionary parameter $\mathscr{T}_m(t)$ or $\mathscr{T}_k(t)$ as

$$t\frac{\partial}{\partial t} = \frac{1}{3}\mathscr{T}_{m,k}\frac{\partial}{\partial \mathscr{T}_{m,k}} \tag{24}$$

Alternatively, time-dependence of the hydraulic fracture can be described in terms of either of the dimensionless times $\tau_{m,k}=\mathscr{T}_{m,k}^3$, which can be further written via the viscosity t_m and the toughness t_k timescales as

$$\tau_{m,k} = \frac{t}{t_{m,k}} \qquad \text{with } t_m = \frac{E'^3}{\left(-p_{\mathrm{t}}\right)^3}\frac{\mu'}{E'}, \quad t_k = \frac{E'^3}{\left(-p_{\mathrm{t}}\right)^3}\frac{K'^4}{E'^4 Q_o} \tag{25}$$

Dimensionless parameters and field quantities in the two scalings bear a simple relation

$$\mathscr{M}_k = \mathscr{K}_m^{-4}, \quad \mathscr{T}_k = \mathscr{K}_m^{-4/3}\mathscr{T}_m \tag{26}$$

$$\frac{\gamma_{\mathrm{f}k}}{\gamma_{\mathrm{f}m}} = \frac{\gamma_k}{\gamma_m} = \frac{L_m}{L_k} = \mathscr{K}_m^{2/3}, \quad \frac{\Pi_k}{\Pi_m} = \frac{\epsilon_m}{\epsilon_k} = \mathscr{K}_m^{-4/3}, \quad \frac{\Omega_k}{\Omega_m} = \mathscr{K}_m^{-2/3} \tag{27}$$

Similitude between any two-*dimensional* solutions of hydraulic fracture is achieved when dimensionless toughness $\mathscr{K}_m$ is invariant and the ranges of dimensionless time-dependent stress of the two solutions are the same.

Table 1
Scaling factors ϵ and L and dimensionless groups $\mathscr{M}$, $\mathscr{K}$, and $\mathscr{T}$ in the viscosity and the toughness scalings

	Viscosity-scaling	Toughness-scaling
L	$L_m = \left(\frac{E'^{1/4} Q_o^{3/4} t}{\mu'^{1/4}}\right)^{2/3}$	$L_k = \left(\frac{E' Q_o t}{K'}\right)^{2/3}$
ε	$\varepsilon_m = \left(\frac{\mu'}{E' t}\right)^{1/3}$	$\varepsilon_k = \left(\frac{K'^4}{E'^4 Q_o t}\right)^{1/3}$
$\mathscr{M}$	$\mathscr{M}_m = 1$	$\mathscr{M}_k = \frac{E'^3 Q_o \mu'}{K'^4}$
$\mathscr{K}$	$\mathscr{K}_m = \frac{K'}{E'^{3/4} Q_o^{1/4} \mu'^{1/4}}$	1
$\mathscr{T}$	$\mathscr{T}_m = \frac{-p_t}{E'} \left(\frac{E' t}{\mu'}\right)^{1/3}$	$\mathscr{T}_k = \frac{-p_t}{E'} \left(\frac{E'^4 Q_o t}{K'^4}\right)^{1/3}$

Indices 'm' and 'k' are used to identify quantities in the two respective scalings.

3.3. Propagation regimes

Limiting propagation regimes of the fluid-driven fracture with a lag can be defined in terms of a pair of dimensionless numbers: toughness $\mathscr{K}_m$ and underpressure $\mathscr{T}_m$ in the viscosity scaling, or viscosity $\mathscr{M}_k$ and underpressure $\mathscr{T}_k$ in the toughness scaling. Number $\mathscr{K}_m$ or $\mathscr{M}_k$ defines the balance between the two energy dissipation mechanisms corresponding to the fracturing of the solid and to the flow of viscous fluid in the fracture channel. In the limit when $\mathscr{K}_m \ll 1$, fracture propagation is dominated by the dissipation in the fluid (propagation along a preexisting discontinuity), while in the limit $\mathscr{M}_k \ll 1$, the fracture propagation is dominated by solid toughness (the inviscid fluid approximation).

The dimensionless underpressure $\mathscr{T}_{m,k}$ is naturally linked to the existence of a non-zero lag, since when the lag is zero, the fluid and fracture fronts coincide, the pressure boundary condition at the fluid front, Eq. (18) or (5), is no longer applicable, and the fluid pressure at the fracture tip is the part of the solution. Since $\mathscr{T}_{m,k}$ is the only parameter which embodies the confining stress, Eq. (23), the solution for the net-pressure (fluid pressure minus the confining stress) under the zero lag condition is independent of the confining stress. Limiting conditions which correspond to the vanishing fluid lag $1 - \xi_f$ and, on the opposite end, vanishing fluid fraction ξ_f can be identified from the following considerations.

- Fluid lag vanishes in the zero viscosity limit $\mathscr{M}_k \to 0$ ($\mathscr{K}_m \to \infty$). Indeed, lubrication equation (17) suggests that the pressure gradient vanishes with $\mathscr{M}_k$, $\partial \Pi_k / \partial \zeta = \mathrm{O}(\mathscr{M}_k)$, everywhere along the fluid-filled part of the fracture. If the lag does not simultaneously vanish, then by continuity at the fluid front, Eq. (18), the net-pressure in the crack is uniform and is equal to the negative value $(-\mathscr{T}_k)$ in the lag. The latter would imply negative crack opening, and, therefore, contradicts the assumption of an open partially fluid-filled crack.
- Similarly, fluid lag has to vanish in the limit of infinitely large underpressure $\mathscr{T}_{k,m} \to \infty$, since otherwise it would incur diverging pressure in the fluid-filled part, $\Pi_{k,m} \to \infty$, to insure positiveness of crack opening, Eq. (20), and validity of the fracture propagation criteria (22).
- Consistently with the above, the lag is a decreasing function of both underpressure $\mathscr{T}_m$ and toughness $\mathscr{K}_m$ parameters: for a constant value of dimensionless toughness $\mathscr{K}_m$, the maximum value of the lag corresponds to the zero underpressure limit.
- In the zero underpressure limit, the lag spans entire crack, $1 - \xi_f \to 1$, (i.e. fluid fraction vanishes, $\xi_f \to 0$) when toughness is zero $\mathscr{K}_m \to 0$, and the lag is zero $1 - \xi_f \to 0$ (i.e. the fracture is fully fluid-filled, $\xi_f \to 1$) when toughness is infinite $\mathscr{K}_m \to \infty$ (or viscosity is zero $\mathscr{M}_k \to 0$). To demonstrate the former, consider the case when the effects of the underpressure and the toughness are small (in the viscosity scaling: $\mathscr{T}_m \ll 1$ and $\mathscr{K}_m \ll 1$). Pressure Π in the channel monotonically decreases with the distance form the inlet and attains its minimum value $(-\mathscr{T}_m)$ at the fluid front, Eq. (18). Vanishing tip underpressure, therefore, implies that the pressure Π_m is non-negative, and, furthermore, is not everywhere zero in order for the crack to be open and to accommodate the volume of injected fluid, Eq. (19). Consequently, the integral in the right side

of Eq. (22) is positive O(1) constant, which has to be balanced by either the toughness term in the left side of Eq. (22), $O(\mathscr{K}_m/\xi_f^{1/2})$, or by the underpressure term in the right side of Eq. (22), $O(\mathscr{T}_m/\xi_f)$. Thus, the fluid fraction vanishes, $\xi_f \to 0$, as the larger of the two vanishing parameters:

$$\xi_f = \begin{cases} O(\mathscr{K}_m^2), & \mathscr{T}_m \leqslant \mathscr{K}_m^2 \ll 1 \\ O(\mathscr{T}_m), & \mathscr{K}_m^2 \leqslant \mathscr{T}_m \ll 1 \end{cases} \tag{28}$$

Zero toughness, zero underpressure limit corresponds to an unstable fracture which is neither confined by the underpressure in the lag region, nor does the solid has any resistance to its propagation. Such that upon application of an infinitesimal fluid loading via fluid injection at the inlet the fracture tends to "run away" infinitely fast. Since flow of viscous fluid can commence only at a finite velocity for finite pressure gradients, fluid front in the fracture lags significantly behind the front of the run-away fracture. When the toughness and the underpressure parameters are small (but at least one of them is non-zero), the fracture propagates with large but finite velocity and the injected fluid forms a boundary layer near the fracture inlet. On the lengthscale of the fracture (i.e. away form the inlet fluid boundary layer), fracture loading can thus be approximated by a pair of net point-forces applied at the fracture origin.

Based on the discussion above, the normalized solution for the fluid-driven fracture propagation with a lag in an elastic medium can be represented in the so-called MKO parametric diagram (Fig. 2). The OK and MK edges of the diagram correspond to the zero underpressure/time ($\mathscr{T}_{m,k} = 0$) and infinite underpressure/time ($\mathscr{T}_{m,k} = \infty$) asymptotic limits, while the OM edge and the K-vertex correspond to the viscosity-dominated (zero toughness) and toughness-dominated (zero viscosity) limits, respectively. Solution trajectories in the MKO space, characterized by a given value of dimensionless toughness $\mathscr{K}_m$ (or viscosity $\mathscr{M}_k$), originate from the OK edge where the lag is maximum and evolve towards the MK edge where the lag vanishes. In the toughness-dominated regime ($\mathscr{M}_k = 0$) the trajectory reduces to a point (K-vertex) since the lag is zero for any value of underpressure and no evolution of the normalized solution is taking place.

The beginning (zero underpressure limit, the OK edge) and the end (zero lag limit, the MK edge) of the fracture evolution correspond to the self-similar solutions of the respective time-independent limits of the normalized equations (17)–(22), so that the time dependence of *dimensional* opening, pressure, lag, and crack length are defined by that of the respective scaling, see Eqs. (12) and Table 1. The zero-lag solution of Spence and Sharp (1985) provides solution for the MK-edge, while the behavior of the solution at and near the M- and K-vertices along this edge has been investigated by Carbonell et al. (1999), Adachi and Detournay (2002), Garagash and Detournay (2002, 2005), and Garagash (2000, in press), respectively. The OK-edge solution and

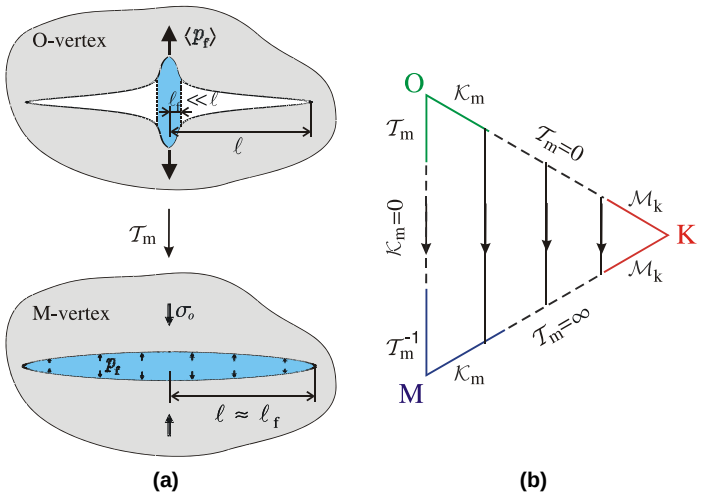

Fig. 2. (a) Schematic evolution of the fracture in the zero toughness case (OM-edge). (b) Parametric space MKO for a plane-strain fluid-driven fracture in an elastic solid under the condition of zero fluid leak-off.

its behavior near the O- and K-vertices is the focus of this paper. This solution provides the initial condition for the transient solution in the MKO triangle and together with the MK-edge solution provides asymptotic bounds on the important fracture variables (length, lag, etc.).

4. Asymptotic solutions

4.1. Small tip underpressure, small toughness solution (O-corner)

In this section we consider solution regime characterized by small underpressure/time $\mathscr{T}_m \ll 1$ and small toughness $\mathscr{K}_m \ll 1$, corresponding to the vicinity of O-vertex in the MKO parametric space, Fig. 2. Per preceding discussion, O-vertex is singular as it corresponds to a non-physical limit of zero resistance to fracture and zero underpressure in the lag. However, solution in the vicinity of the vertex when at least one of the two parameters $\{\mathscr{T}_m, \mathscr{K}_m\}$ is non-zero has a clear physical meaning corresponding to a fluid-driven fracture propagating in the solid of low toughness, or driven by fluid of high viscosity, and either under low tip underpressure, or at early time. It is expected that in this small underpressure, small toughness regime, fluid invades only a small fraction of the fracture length $\xi_f \ll 1$, and that the extent of this "fluid boundary layer" (BL) at the crack inlet scales with the larger of the two parameters: $\mathscr{T}_m$ and $\mathscr{K}_m^2$, Eq. (28).

Governing equations for the fluid-driven fracture in viscosity scaling are given by Eqs. (17)–(22) and Table 1. The solution strategy is to expand the solution in the fluid BL, inner expansion, and away from the BL, outer expansion, in a small unknown fluid fraction $\xi_f \ll 1$. Using these expansions in the fracture propagation condition will then provide the solution for ξ_f.

Elasticity expression (20) for the opening allows the following inner and outer expansions in the small parameter ξ_f:

$$\zeta = \mathrm{O}(1): \quad \bar{\Omega}_{fm} = \epsilon_f^{-1}\langle \Pi_m \rangle + \omega_m(\zeta) - 4\frac{\mathscr{T}_m}{\xi_f} + \cdots \tag{29}$$

$$\xi = \mathrm{O}(1): \quad \bar{\Omega}_{fm} = G(\xi, 0)\langle \Pi_m \rangle - 4\frac{\mathscr{T}_m}{\xi_f}(1-\xi^2)^{1/2} + \cdots \tag{30}$$

respectively. In the above, ϵ_f is a logarithmically small quantity

$$\epsilon_f = \frac{\pi}{8\ln(2/\xi_f)} \tag{31}$$

while the average net-pressure in the fluid boundary layer, $\langle \Pi_m \rangle$, and the function $\omega_m(\zeta)$ are defined as follows:

$$\langle \Pi_m \rangle = \int_0^1 \Pi_m \, \mathrm{d}\zeta, \quad \omega_m(\zeta) = -\frac{4}{\pi}\int_0^1 \ln \mid \zeta^2 - \zeta'^2 \mid \Pi_m(\zeta')\,\mathrm{d}\zeta' \tag{32}$$

Similar expansion of the propagation condition (22) yields

$$\frac{\pi}{2^{7/2}}\frac{\mathscr{K}_m}{\xi_f^{1/2}\gamma_f^{1/2}} = \langle \Pi_m \rangle - \frac{\pi}{2}\frac{\mathscr{T}_m}{\xi_f} + \cdots \tag{33}$$

(Note that truncated terms in Eq. (29) and Eqs. (30) and (33) are $\mathrm{O}(\epsilon_f^{-1}\mathscr{T}_m, \gamma_f \Pi_m \xi_f^2)$ and $\mathrm{O}(\mathscr{T}_m, \Pi_m \xi_f^2)$, respectively).

As anticipated from the scaling, the leading term in the fracture opening away from the inlet, Eq. (30), is given by the solution for a crack loaded by a pair of point forces $\langle \Pi_m \rangle$ at the origin. Expansion of the opening in the inlet BL, Eq. (29), involves logarithmically large quantity ϵ_f^{-1}, Eq. (31), which is consistent with the logarithmic singularity in the outer expansion (30) if extended to the fracture inlet.[3]

Based on inner expansion (29), global fluid continuity (19) and lubrication (17) equations, we can obtain the following estimates for the BL solution: $\bar{\Omega}_{fm} = \mathrm{O}(\epsilon_f^{-1}\Pi_m)$, $\gamma_{fm} = \mathrm{O}(\bar{\Omega}_m^{-1/2})$, and $\Pi_m = \mathrm{O}(\bar{\Omega}_f^{-2})$, respectively.

[3] Term $G(\xi, 0)$ in (30) is logarithmically singular at $\xi = 0$, see Eq. (8).

(The latter estimate ensures a non-trivial solution with non-zero pressure gradient in the BL.) These BL estimates can be rewritten in terms of the logarithmically small parameter ϵ_f as

$$\zeta = O(1): \qquad \bar{\Omega}_{fm} = O(\epsilon_f^{-1/3}), \quad \gamma_{fm} = O(\epsilon_f^{1/6}), \quad \Pi_m = O(\epsilon_f^{2/3}) \tag{34}$$

Using the pressure estimate $(34)_c$ in Eq. (30), the opening away from the inlet BL is $\Omega_m = O(\epsilon_f^{2/3})$.

According to Eq. $(34)_c$, the pressure in the BL can be expanded in ϵ_f:

$$\Pi_m(\zeta) = \epsilon_f^{2/3}(\Pi_0(\zeta) + O(\epsilon_f)) \tag{35}$$

Propagation condition (33) and non-negative toughness $\mathcal{K}_m \geqslant 0$ require that $\langle \Pi_m \rangle \geqslant \frac{\pi}{2}(\mathcal{T}_m/\xi_f)$. Consequently, the 2nd and the 3rd terms in inner expansion (29) are logarithmically small compared to the 1st term. Then, *to the leading order* in ϵ_f, Eqs. (29) and (19) with the help of Eq. (35) yield

$$\zeta = O(1): \quad \bar{\Omega}_{fm} = \frac{\langle \Pi_0 \rangle}{\epsilon_f^{1/3}} \tag{36}$$

$$\gamma_{fm} = \frac{\epsilon_f^{1/6}}{2^{1/2}\langle \Pi_0 \rangle^{1/2}}, \tag{37}$$

respectively. In the above, $\langle \Pi_0 \rangle$ is the average of $\Pi_0(\zeta)$ over the BL, $\langle \Pi_0 \rangle = \int_0^1 \Pi_0 \, d\zeta$.

The leading order expressions in the BL, Eqs. (36), (37), agree with estimates (34) and also imply that the opening in the BL to the leading order is a constant. Applying Eqs. (35)–(37) to the lubrication equation (17) with Table $1_{(m)}$, upon some algebra, neglecting small terms originating from the evolution terms (24) in Eq. (17), such as $(\mathcal{T}_m/\epsilon_f)(d\epsilon_f/d\mathcal{T}_m) = \frac{8}{\pi}\epsilon_f(\mathcal{T}_m/\xi_f)(d\xi_f/d\mathcal{T}_m) = O(\epsilon_f)$, and integrating in ζ yields

$$\frac{1}{2}(1-\zeta)^2 + \frac{1}{3}\left[1 - \frac{1}{4}\frac{\mathcal{T}_m}{\langle \Pi_0 \rangle}\frac{d\langle \Pi_0 \rangle}{d\mathcal{T}_m}\right](1-\zeta^2) = \langle \Pi_0 \rangle^2(\Pi_0(\zeta) - \Pi_0(1)) \tag{38}$$

According to the condition (18) at the fluid front and Eq. (35), $\Pi_0(1) = -\epsilon_f^{-2/3}\mathcal{T}_m$ is small ($\mathcal{T}_m \ll 1$) and can be neglected to the leading order. Thus, given average pressure value $\langle \Pi_0 \rangle$, Eq. (38) with $\Pi_0(1) = 0$ specifies quadratic variation of the normalized pressure in the fluid lag from zero value at the fluid front, $\zeta = 1$, to the maximum value at the inlet, $\zeta = 0$. To obtain $\langle \Pi_0 \rangle$, we integrate Eq. (38) with $\Pi_0(1) = 0$ over the BL, $0 \leqslant \zeta \leqslant 1$,

$$7 - \frac{\mathcal{T}_m}{\langle \Pi_0 \rangle}\frac{d\langle \Pi_0 \rangle}{d\mathcal{T}_m} = 18\langle \Pi_0 \rangle^3 \tag{39}$$

The above evolution equation admits general solution in terms of the underpressure $\mathcal{T}_m$ and an integration constant: $\langle \Pi_0 \rangle^3 = 7\mathcal{T}_m^{21}/(\text{const} + 18\mathcal{T}_m^{21})$. The choice of integration constant, const $= 0$, follows from the requirement of non-trivial (i.e. non-zero) solution in the zero underpressure limit $\mathcal{T}_m = 0$ whenever toughness $\mathcal{K}_m$ is non-zero. Thus,

$$\langle \Pi_0 \rangle = \left(\frac{7}{18}\right)^{1/3} \tag{40}$$

and normalized pressure in the BL defined by Eq. (38) with $\Pi_0(1) = 0$ is time independent.

Consequently, dependence of the BL solution (35), (36) on underpressure $\mathcal{T}_m$ and toughness $\mathcal{K}_m$ is only through that of the parameter ϵ_f, or, equivalently, that of the fluid fraction ξ_f, see Eq. (31). To find the fluid fraction ξ_f, we substitute leading-order-expressions $\langle \Pi_m \rangle = \epsilon_f^{2/3}\langle \Pi_0 \rangle$, Eq. (35), and Eq. (37) with Eqs. (40) and (31) into the propagation condition (33) to find:

$$\left(\frac{9\pi}{56}\right)^{\frac{1}{4}}\left(\ln\frac{2}{\xi_f}\right)^{\frac{3}{4}}\frac{\mathcal{K}_m}{\xi_f^{1/2}} + \left(\frac{144\pi}{7}\right)^{\frac{1}{3}}\left(\ln\frac{2}{\xi_f}\right)^{\frac{2}{3}}\frac{\mathcal{T}_m}{\xi_f} = 1 \tag{41}$$

Eq. (41) provides the fluid fraction ξ_f as an implicit function of $\mathcal{T}_m$ and $\mathcal{K}_m$. In the limit when either $\mathcal{K}_m$ or $\mathcal{T}_m$ is zero, an explicit expression for the fluid fraction as a function of remaining non-zero parameter can be obtained from (41)

$$\mathcal{T}_m = 0: \qquad \xi_f = 2\bar{\mathcal{K}}_m^2[\mathrm{W}(\bar{\mathcal{K}}_m^{-4/3})]^{3/2}, \quad \bar{\mathcal{K}}_m = \left(\frac{243\pi}{1792}\right)^{1/4}\mathcal{K}_m \tag{42}$$

$$\mathcal{K}_m = 0: \qquad \xi_f = 2\bar{\mathcal{T}}_m[\mathrm{W}(\bar{\mathcal{T}}_m^{-3/2})]^{2/3}, \quad \bar{\mathcal{T}}_m = \left(\frac{8\pi}{7}\right)^{1/3}\mathcal{T}_m \tag{43}$$

where $w = W(z)$ is the Lambert product log function (defined as the solution of equation $z = we^w$). The two limiting solutions (42) and (43) correspond to the small-toughness (zero underpressure or time) and small-underpressure (zero toughness) solutions in the vicinity of the O-corner of the parametric diagram (Fig. 2b). In Eqs. (42), (43), power-laws of the Lambert function correspond to a small logarithmic correction to the otherwise simple quadratic, $\xi_f \sim \mathcal{K}_m^2$, and linear, $\xi_f \sim \mathcal{T}_m$, asymptotic dependencies, respectively.

Evolution of the fluid fraction with the small underpressure/time $\mathcal{T}_m$ for various values of the small toughness $\mathcal{K}_m$, Eq. (41), is illustrated in Fig. 3 in the log–log scale. It can be noted that the zero toughness solution (43) serves as an envelop for the small non-zero toughness solution (Fig. 3), i.e. provides its intermediate underpressure asymptote.

In summary, the asymptotic small toughness, small underpressure/time solution is given by the implicit expression (41) for the small fluid fraction ξ_f, and the fracture length $\gamma_m = \gamma_{fm}/\xi_f$, pressure Π_m and opening $\Omega_m = \gamma_{fm}\bar{\Omega}_{fm}$ are expressed below in terms of the crack coordinate $\xi = \xi_f\zeta$, respectively,

$$\gamma_m = \frac{1}{\xi_f}\left(\frac{9\varepsilon_f}{28}\right)^{1/6}, \quad \left(\epsilon_f = \frac{\pi}{8\ln(2/\xi_f)}\right) \tag{44}$$

$$\Pi_m(\xi) = H(\xi - \xi_f)\left(\frac{18\varepsilon_f}{7}\right)^{\frac{2}{3}}\left(\frac{1}{2}\left(1 - \frac{\xi}{\xi_f}\right)^2 + \frac{1}{3}\left(1 - \frac{\xi^2}{\xi_f^2}\right)\right) \tag{45}$$

$$\xi \gg \xi_f: \quad \Omega_m(\xi) = \left(\frac{7\varepsilon_f^5}{144}\right)^{\frac{1}{6}}\frac{4}{\pi}\ln\left(\frac{1 + (1-\xi^2)^{1/2}}{1 - (1-\xi^2)^{1/2}}\right) \tag{46}$$

$$\xi \sim \xi_f: \quad \Omega_m(\xi) = \left(\frac{7}{144\varepsilon_f}\right)^{1/6} \tag{47}$$

where $H(\cdot)$ denotes the Heaviside step function.

4.2. Small viscosity solution (K-corner)

According to the discussion in Section 3.3, the K-vertex solution corresponds to the limit of inviscid fluid $\mathcal{M}_k = 0$, or, equivalently, of infinite toughness $\mathcal{K}_m = \mathcal{M}_k^{-1/4}$, Eq. (26). Since the fluid lag vanishes in this limit,

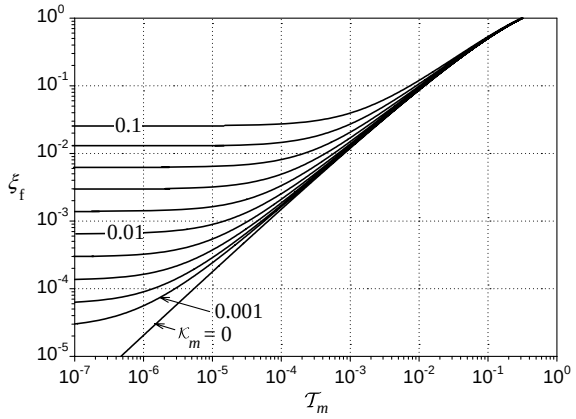

Fig. 3. Evolution of the fluid fraction ξ_f with the dimensionless tip underpressure $\mathcal{T}_m$ for different values of dimensionless toughness $\mathcal{K}_m$ in the small underpressure, small toughness solution (O-corner).

the K-vertex solution is self-similar, i.e., independent of the underpressure $\mathscr{T}_k$. The K-vertex solution in the toughness-scaling can be established from the governing equations (A.1)–(A.6) with Table $1_{(k)}$ and $\mathscr{M}_k = 0$ in the following form (Garagash, in press, Eq. (32)):

$$\Pi_{k0} = \frac{\pi^{1/3}}{8}, \quad \bar{\Omega}_{k0} = \frac{\pi^{1/3}}{2}\sqrt{1-\xi^2}, \quad \gamma_{k0} = \frac{2}{\pi^{2/3}}, \quad \xi_{f0} = 1 \tag{48}$$

(Note that the pressure boundary condition at the fluid front, Eq. (A.2), $\Pi_k(\xi_f) = -\mathscr{T}_k$, is based on the considerations for, however, small but non-zero lag, i.e. $\xi_f < 1$, and, therefore is inconsequential in the case when the lag is exactly zero, $\xi_f = 1$.) When dimensionless viscosity is small but non-zero, $\mathscr{M}_k \ll 1$, the fluid lag is also small but non-zero and the pressure boundary condition at the fluid front is, therefore, violated. This points to the existence of the near tip boundary layer encompassing the fluid lag. Consequently, the small viscosity solution (K-corner) has to consist of the zero lag outer solution, away from the tip BL, and of the near tip BL solution accounting for the effect of the lag. In the following we briefly recapitulate the zero-lag outer solution of Garagash (in press) and then discuss the near tip BL solution and its matching with the outer solution.

Outer solution. The outer solution is given by the series expansion in small $\mathscr{M}_k$,

$$\gamma_k = \gamma_{k0} + \mathscr{M}_k\gamma_{k1} \quad \Pi_k = \Pi_{k0} + \mathscr{M}_k\Pi_{k1} \quad \bar{\Omega}_k = \bar{\Omega}_{k0} + \mathscr{M}_k\bar{\Omega}_{k1} \tag{49}$$

governed by Eqs. (A.1)–(A.6) with Table $1_{(k)}$ and $\xi_f = 1$ (zero lag in the outer solution). (Note that the assumption of zero lag in the outer $O(\mathscr{M}_k)$ solution, Eq. (49), implies that the lag is the higher order term in $\mathscr{M}_k$, which is further validated from the matching of the outer and the lag BL solutions.) The first term of the outer expansion is given by the K-vertex solution (48). The next-order term is in the form (Garagash, in press, Eqs. (40)–(42))

$$\gamma_{k1} = -\frac{32(1+6\ln 2)}{9\pi^{5/3}} \tag{50}$$

$$\Pi_{k1} = \frac{8}{3\pi^{2/3}}\left(\frac{1}{24} + \ln\left(4\sqrt{1-\xi^2}\right) - \frac{3}{4}\frac{\xi\arccos\xi}{\sqrt{1-\xi^2}}\right) \tag{51}$$

$$\bar{\Omega}_{k1} = \frac{8}{3\pi^{2/3}}\left(2\pi - 4\xi\arcsin\xi - \left(\frac{5}{6} - \ln 2\right)\sqrt{1-\xi^2} - \frac{3}{2}\ln\left[\frac{\left(1+\sqrt{1-\xi^2}\right)^{1+\sqrt{1-\xi^2}}}{\left(1-\sqrt{1-\xi^2}\right)^{1-\sqrt{1-\xi^2}}}\right]\right) \tag{52}$$

It is worth noting that the outer solution (49) with Eqs. (48) and (50)–(52) is "outer" in the net-pressure only, since its expression for the opening satisfies the near tip square root asymptote for the opening in the toughness scaling $\bar{\Omega}_k = \gamma_k^{-1/2}(1-\xi)^{1/2}$, Eq. (A.5) with Table $1_{(k)}$, and, therefore, uniformly valid along the fracture length (including the tip BL). The near tip asymptote of the outer solution for the net-pressure following from Eq. (51) is

$$1-\xi \ll 1: \quad \Pi_k = \frac{\pi^{1/3}}{8} + \mathscr{M}_k\frac{4}{3\pi^{2/3}}\left(\ln(1-\xi^2) + 4\ln 2 - \frac{17}{12}\right) \tag{53}$$

Boundary layer solution. Given that the fluid lag boundary layer is sufficiently small, it can be safely assumed to belong entirely to the vicinity of the fracture tip where opening is dominated by the LEFM square root asymptote $\bar{\Omega}_k = \gamma_{k0}^{-1/2}(1-\xi)^{1/2}$ $(1-\xi \ll 1)$, see Eq. (A.5) with Table $1_{(k)}$. On the other hand, to the leading order in $\mathscr{M}_k$, lubrication equation (A.1) in the fluid-filled part $(1-\xi_f \leqslant 1-\xi \ll 1)$ of the tip BL is $(2/3)\mathscr{M}_k\bar{\Omega}_k^{-2} = -\partial\Pi_k/\partial\xi$. Integration of the latter using the fluid front condition $\Pi_k(\xi_f) = -\mathscr{T}_k$, yields the net pressure distribution in the tip BL

$$1-\xi \ll 1: \quad \Pi_k = -\mathrm{H}(\xi-\xi_f)\mathscr{T}_k + \mathrm{H}(\xi_f-\xi)\mathscr{M}_k\frac{2\gamma_{k0}}{3}\ln\frac{1-\xi}{1-\xi_f} \tag{54}$$

Extent of the fluid lag is obtained from matching the BL solution (54) with the near tip asymptote (53) of the outer solution as follows:

$$1-\xi_{\mathrm{f}}=\exp\left[-\frac{3\pi^{2/3}}{4}\left(\frac{\pi^{1/3}}{8}+\mathscr{T}_k\right)\mathscr{M}_k^{-1}-\left(5\ln 2-\frac{17}{12}\right)\right] \tag{55}$$

Composite solution. Expression (55) suggests that the lag is exponentially small for $\mathscr{M}_k \ll 1$ and is, indeed, inconsequential in the outer solution.[4] That is the composite small viscosity solution valid over the entire crack length is given by the outer solution (49) with the provision that the net-pressure is equal to $-\mathscr{T}_k$ over the exponentially small lag, Eq. (55), namely,

$$\gamma_k=\gamma_{k0}+\mathscr{M}_k\gamma_{k1} \tag{56}$$
$$\Pi_k=\mathrm{H}(\xi_{\mathrm{f}}-\xi)(\Pi_{k0}+\mathscr{M}_k\Pi_{k1})-\mathrm{H}(\xi-\xi_{\mathrm{f}})\mathscr{T}_k \tag{57}$$
$$\bar{\Omega}_k=\bar{\Omega}_{k0}+\mathscr{M}_k\bar{\Omega}_{k1} \tag{58}$$

where various terms can be found in Eqs. (48), (51), (50) and (55).

The small viscosity (large toughness) solution (56)–(58) corresponds to the $\mathrm{O}(\mathscr{M}_k)$ correction to the K-vertex solution (48) characterized by the uniform distribution of the net-pressure and the classical square-root opening profile. For a detailed discussion of the identical (except for the exponentially small lag) small viscosity solution in the limit of infinite underpressure $\mathscr{T}_k \to \infty$ (i.e. solution in the vicinity of the K-vertex along the zero lag MK-edge) the reader is referred to Garagash (in press).

4.3. Asymptotic solution along the OK-edge (zero underpressure/time)

Consider now the "beginning" of the fluid-driven fracture evolution which corresponds to a point on the OK-edge of the MKO parametric space (Fig. 2). In the corresponding zero underpressure limit, $\mathscr{T}_m=0$, normalized governing equations expressed in terms of the crack coordinate ξ, Eqs. (A.1)–(A.6) in the viscosity scaling, Eqs. (12) with Table $1_{(m)}$, reduce to the following self-similar set of equations defined over the extent of the fluid channel, $0\leqslant\xi\leqslant\xi_{\mathrm{f}}$:

$$\int_{\xi}^{\xi_{\mathrm{f}}}\bar{\Omega}_m\,\mathrm{d}\xi+\frac{2}{3}\xi\bar{\Omega}_m=-\bar{\Omega}_m^3\frac{\mathrm{d}\Pi_m}{\mathrm{d}\xi},\quad \Pi_m(\xi_{\mathrm{f}})=0 \tag{59}$$
$$\gamma_m^{-2}=2\int_0^{\xi_{\mathrm{f}}}\bar{\Omega}_m\,\mathrm{d}\xi \tag{60}$$
$$\bar{\Omega}_m(\xi)=\int_0^{\xi_{\mathrm{f}}}G(\xi,\xi')\Pi_m(\xi')\,\mathrm{d}\xi' \tag{61}$$
$$\mathscr{K}_m=\frac{2^{7/2}}{\pi}\gamma_m^{1/2}\int_0^{\xi_{\mathrm{f}}}\frac{\Pi_m\,\mathrm{d}\xi}{(1-\xi^2)^{1/2}}\quad\text{or}\quad 1-\xi\ll 1:\bar{\Omega}_m=\mathscr{K}_m\gamma_m^{-1/2}(1-\xi)^{1/2} \tag{62}$$

where $\bar{\Omega}_m=\Omega_m/\gamma_m$. (In the order of appearance: lubrication combined with the pressure condition at the fluid interface, global fluid continuity, elasticity and propagation condition.) The corresponding zero underpressure/time self-similar solution $\mathscr{F}_m(\xi,\mathscr{T}_m=0,\mathscr{K}_m)=\{\Omega_m,\Pi_m,\gamma_m,\xi_{\mathrm{f}}\}$ of Eqs. (59)–(62) is the function of the constant dimensionless toughness $\mathscr{K}_m$, and the crack coordinate ξ. The time-dependence of the dimensional opening, pressure, crack length, and fluid channel length is given solely by that of the viscosity scaling parameters, Table $1_{(m)}$.

The OK-edge solution near the O- or K-vertices when $\mathscr{K}_m \ll 1$ and $\mathscr{K}_m \gg 1$, respectively, is given by the corresponding analytical asymptotic solutions discussed in previous sections. The OK-edge finite toughness solution, which corresponds to the case when neither the fluid-invaded part of the crack nor the lag are vanishingly small, is obtained herein numerically. To avoid solving governing equations in an a priori unknown domain (bounded by unknown fluid boundary $\xi=\xi_{\mathrm{f}}(\mathscr{K}_m)$), we postulate a value of ξ_{f} and compute corresponding value

[4] In fact, expression for the lag (55) can be obtained directly from the outer solution requiring that the net-pressure in the outer solution attains value $-\mathscr{T}_m$ at the fluid front $\xi=\xi_{\mathrm{f}}$.

Table 2
Dimensionless toughness parameter $\mathscr{K}_m$, crack length γ_m, net-pressure at the inlet $\Pi_m(0)$, crack opening at the inlet $\Omega_m(0)$, and the numerical error for various values of the fluid fraction ξ_f

ξ_f	$\mathscr{K}_m$	γ_m	$\Pi_m(0)$	$\Omega_m(0)$	$e^{(51)}$
0.0001	0.0020	4740.0	0.163	1.113	4.79×10^{-7}
0.001	0.0076	492.55	0.189	1.085	3.46×10^{-7}
0.01	0.0306	51.767	0.229	1.055	1.31×10^{-6}
0.03	0.0616	17.781	0.258	1.040	3.16×10^{-6}
0.1	0.139	5.553	0.302	1.025	8.75×10^{-6}
0.2	0.230	2.855	0.338	1.020	1.69×10^{-5}
0.3	0.317	1.939	0.365	1.019	2.66×10^{-5}
0.4	0.405	1.474	0.389	1.021	3.88×10^{-5}
0.5	0.498	1.192	0.412	1.026	5.53×10^{-5}
0.6	0.600	1.002	0.434	1.034	7.92×10^{-5}
0.7	0.720	0.864	0.457	1.046	1.18×10^{-4}
0.8	0.869	0.757	0.482	1.064	1.92×10^{-4}
0.9	1.086	0.667	0.514	1.094	4.01×10^{-4}
0.97	1.382	0.601	0.554	1.142	1.64×10^{-4}
0.99	1.591	0.571	0.583	1.178	9.17×10^{-4}
$1-10^{-4}$	2.140	0.511	0.671	1.281	1.58×10^{-2}
$1-10^{-6}$	2.461	0.481	0.737	1.350	1.97×10^{-2}
$1-10^{-8}$	2.692	0.460	0.793	1.405	2.02×10^{-2}

of the parameter $\mathscr{K}_m(\xi_f)$ as a part of the solution. This method allows to, first, solve lubrication equation (59) and elasticity equation (61) for the opening $\bar{\Omega}_m(\xi,\xi_f)$ and the pressure $\Pi_m(\xi,\xi_f)$, and then evaluate fracture length $\gamma_m(\xi_f)$, Eq. (60), and corresponding value of the toughness parameter $\mathscr{K}_m(\xi_f)$, Eq. $(62)_a$. The numerical algorithm, described in details in Appendix B, makes use of a piecewise linear approximation of the net-pressure Π_m along the fluid channel and corresponding analytical approximation for the opening $\bar{\Omega}_m$ resulting from the integration of the elasticity equation (61). Lubrication equation (59) evaluated at a set of collocation points is then used to form an algebraic system of equations for the values of the pressure at the grid points. Numerical error in the solution of lubrication equation (59) is assessed using the following quadratic measure:

$$e^{(N)}=\int_0^1\left[1-\frac{-\bar{\Omega}_m^3\,\frac{\mathrm{d}\Pi_m}{\mathrm{d}\xi}}{\int_\xi^{\xi_f}\bar{\Omega}_m\,\mathrm{d}\xi+\frac{2}{3}\xi\bar{\Omega}_m}\right]^2\mathrm{d}\xi \tag{63}$$

where N is the number of the pressure grid points.

The numerical solution has been carried out using 51 grid points uniformly distributed along the fluid channel, $\xi\in[0,\xi_f]$, for a set of fluid fraction ξ_f values given in Table 2, which also shows corresponding values of the dimensionless toughness parameter $\mathscr{K}_m$, crack length γ_m, net-pressure and opening at the crack inlet, and numerical error. The numerical error increases with the decreasing lag $1-\xi_f$ or, alternatively, with increasing toughness. This behavior is attributed to the emergence of the logarithmic net-pressure profile characterized by large pressure gradient near the crack tip. To ensure the convergence of the method for small values of the lag ($\xi_f>0.99$ in Table 2), logarithmic net-pressure asymptote (53) of the K-vertex solution has been added as a particular term in the net-pressure numerical solution, see Appendix B for details.

5. Results and discussion

In this section, results for the self-similar zero tip underpressure/time solution (the OK-edge) are presented and contrasted to the O- and K-corner analytical asymptotic solutions. In plotting the results, solid lines are used for the OK-edge solution and dashed lines are used for corner solutions.

Fig. 4 shows the fluid fraction ξ_f and the lag $1-\xi_f$ as a function of the dimensionless toughness parameter $\mathscr{K}_m$ in the zero underpressure solution and in the O-corner, Eq. (42), and the K-corner,[5] $1-\xi_f\simeq$

[5] See Eq. (55) with $\mathscr{T}_k=0$ and $\mathscr{M}_k=\mathscr{K}_m^{-4}$.

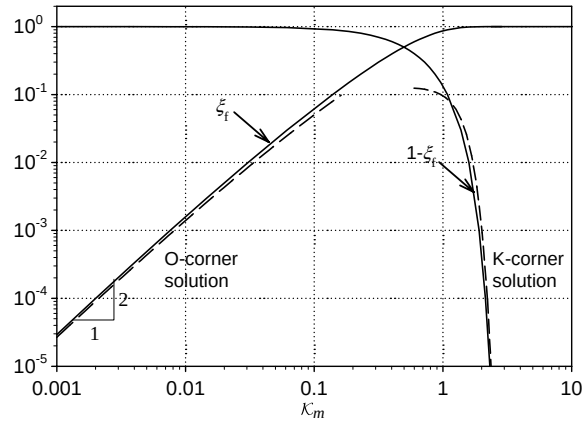

Fig. 4. Self-similar zero tip underpressure solution: the fluid fraction $\xi_f = \ell_f/\ell$ and the lag $1 - \xi_f$ vs. toughness $\mathcal{K}_m$. Solid lines show the numerical OK-edge solution, dashed lines show the small and large toughness asymptotic solutions, corresponding to the O- and K-corners in the parametric space in Fig. 2, respectively.

$0.129 \exp\left[-\frac{3\pi}{32}\mathcal{K}_m^4\right]$, asymptotic solutions. This figure indicates that the lag decreases with toughness from the unity, corresponding to zero fluid fraction, at zero toughness (the O-vertex) to zero at infinite toughness (the K-vertex). Practically, the lag is at least 10% of the crack length for $\mathcal{K}_m < 1$ and is less than 0.1% of the crack length for $\mathcal{K}_m > 2$. The vanishing lag in the latter large-toughness range is well approximated by the K-corner exponential dependence.

Figs. 5 and 6 show the profiles of the dimensionless crack opening and net-pressure along the crack for various values of the fluid front position ξ_f from 10^{-4} to $1 - 10^{-8}$, corresponding to various values of the toughness parameter $\mathcal{K}_m$ from 0.002 to 2.7, respectively (Table 2). Solution for small values of the fluid fraction ξ_f, or, alternatively, for small toughness, is well approximated by the O-corner solution, where the fluid is localized into the inlet boundary layer and the crack opening profile is given by that of a crack loaded by a pair of point forces at the inlet, Eq. (46). Solution for the fluid fraction near unity (small lag, or, alternatively, large toughness) is well approximated by the K-corner solution, where the opening in the zero-order approximation is given by the classical elliptical crack profile $\Omega_m = \mathcal{K}_m^{2/3}\frac{\pi^{1/3}}{2}\sqrt{1-\xi^2}$ (Eq. (48) and scaling relation $(27)_c$).

Fig. 7 shows (a) variation of the dimensionless length γ_m and (b) variation of the dimensionless *inlet* values of the net-pressure $\Pi_m(0)$ and the crack opening $\Omega_m(0)$ with the dimensionless toughness parameter $\mathcal{K}_m$ in the zero underpressure and the infinite underpressure self-similar solutions shown by solid and dotted lines, respectively. The latter solution corresponds to the MK-edge of the MKO parametric diagram where the fluid lag is identically zero. This solution is reproduced in Fig. 7 after Spence and Sharp (1985) and Adachi (2001) in the finite toughness range and after Adachi and Detournay (2002) and Garagash and Detournay (2005) in the small toughness range. The OK- and MK-edge solutions provide asymptotic bounds to the transient solution of hydraulic fracture with the lag. An example of a transient solution trajectory, characterized by a constant value of dimensionless toughness $\mathcal{K}_m = 0.1$, is shown by a thick arrow in Fig. 7: (a) normalized crack length is decreasing by about 1500% in its evolution from small to large underpressure limit; while (b) normalized net-pressure at the inlet is increasing by about 100% and normalized crack opening at the inlet is increasing by about 10%. For larger values of toughness, $\mathcal{K}_m \gtrsim 2$, the small and large underpressure limits become practically identical, as the lag becomes negligibly small in the zero underpressure solution (see discussion of Fig. 4). Furthermore, for values of toughness $\mathcal{K}_m \gtrsim 4$ both solutions are adequately approximated by the K-corner solution (shown by the dashed line in Fig. 7).

The above discussion clearly indicates the prominent effect of the fluid lag on the hydraulic fracture evolution, assessed through the comparative analysis of the small and large time asymptotic solutions, for small enough values of dimensionless toughness parameter $\mathcal{K}_m$. The small and large time asymptotic behavior of physical (dimensional) crack length, net-pressure and opening can be obtained directly from the viscosity scaling (Eqs. (12) with Table $1_{(m)}$).Namely, dimensional crack length $\ell = \gamma_m L_m(t)$ with the lengthscale $L_m \sim t^{2/3}$ (Table 1) evolves from the small time similarity solution $\gamma_m^{(\mathrm{OK-edge})} L_m(t)$ to the large time similarity solution

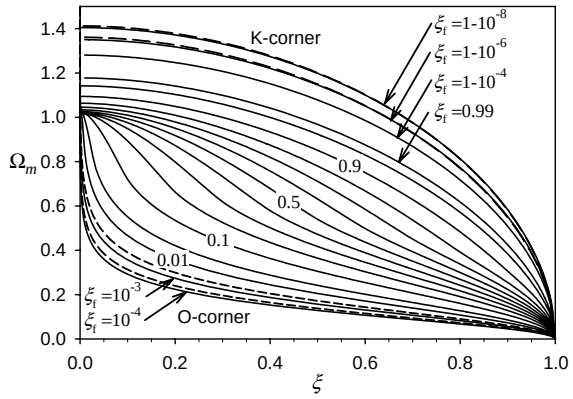

Fig. 5. Self-similar zero tip underpressure solution: the dimensionless opening Ω_m $(= \gamma_m \bar{\Omega}_m)$ along the fracture for various values of the fluid front position ξ_f (corresponding values of toughness $\mathscr{K}_m$ are shown in Table 2).

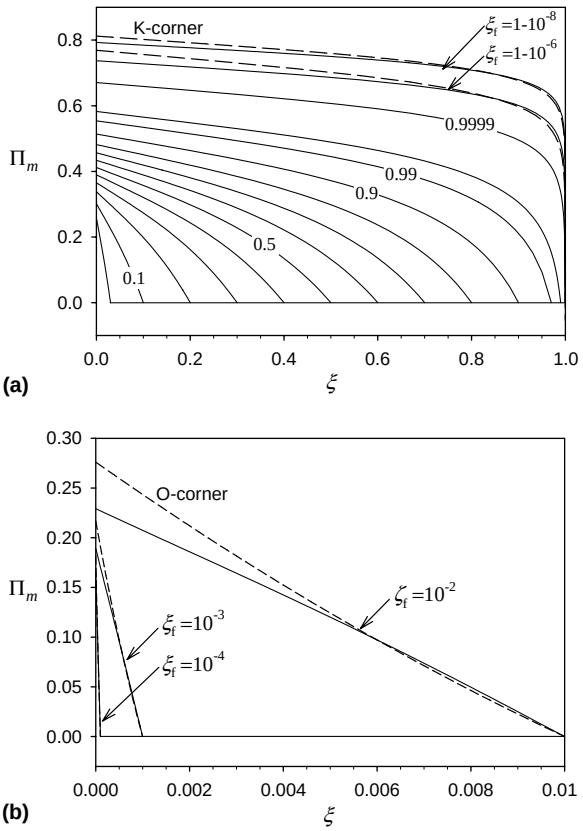

Fig. 6. Self-similar zero tip underpressure solution: the dimensionless net pressure Π_m along the fracture for (a) various values of fluid front position ξ_f and (b) various small values of ξ_f. (See Table 2 for corresponding values of toughness $\mathscr{K}_m$.)

$\gamma_m^{(\mathrm{MK-edge})} L_m(t)$, see the insert of Fig. 7(a). (Note that even though $\gamma_m^{(\mathrm{OK-edge})} > \gamma_m^{(\mathrm{MK-edge})}$, the dimensional length ℓ increases with time due to the increasing lengthscale $L_m(t)$.) Similarly, even though the inlet value of the normalized net-pressure increases from the early to large time limit (Fig. 7(b)), the dimensional net-pressure $p - \sigma_o = \varepsilon_m(t) E' \Pi_m$ with $\varepsilon_m \sim t^{-1/3}$ is decreasing between the small and large time limits.

The data in Fig. 7 are replotted in Fig. 8 to show the dimensionless crack length γ_m, (a), and the inlet crack opening $\Omega_m(0)$, (b), parametrized by the inlet net-pressure $\Pi_m(0)$. Fig. 8(a) together with scaling definitions

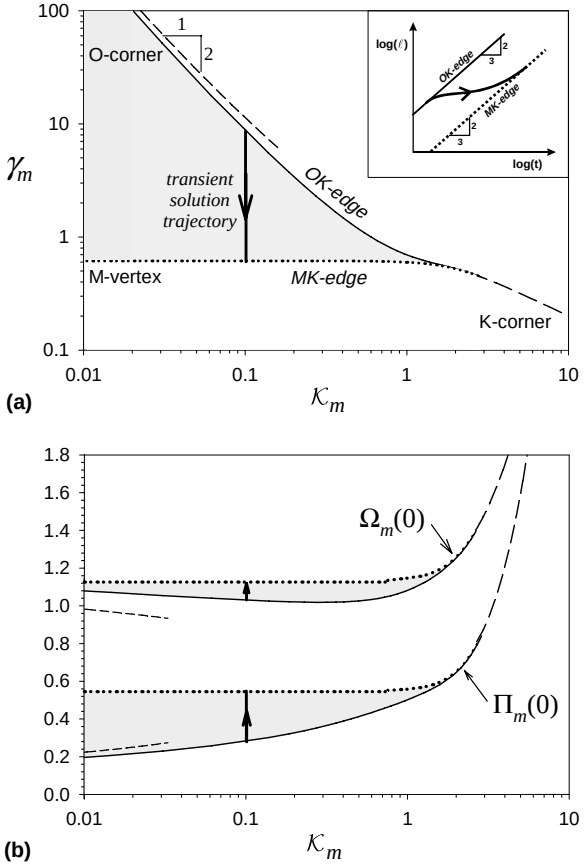

Fig. 7. Self-similar zero tip underpressure solution: the dimensionless fracture length γ_m, (a), and the dimensionless net-pressure $\Pi_m(0)$ and crack opening $\Omega_m(0)$ at the inlet, (b), vs. the dimensionless toughness $\mathcal{K}_m$. Dashed lines show asymptotic O-corner and K-corner solutions. Dotted lines show the self-similar infinite tip underpressure solution (Spence and Sharp, 1985; Adachi, 2001).

(12) and Table 1 can be useful in practice in order to estimate evolving crack length from the monitored evolution of the inlet pressure. Interestingly, the plots corresponding to the zero underpressure solution (solid line) and that to the infinite underpressure solution (dotted line) practically overlap over the entire applicable range of the dimensionless net-pressure ($\Pi_m(0) \geqslant 0.545$). Note that each point on the overlapping curve corresponds to different values of toughness parameter $\mathcal{K}_m$ in the two solutions. For example, the point corresponding to the M-vertex solution (infinite underpressure, zero-toughness solution), see empty circle in Fig. 8, corresponds to the zero underpressure solution with $\mathcal{K}_m \simeq 1.31$. Consequently, an approximate overlap between the two solutions occurs in the range $\mathcal{K}_m \gtrsim 1.31$ of the zero underpressure solution and the range $0 \leqslant \mathcal{K}_m < \infty$ of the infinite underpressure solution. It is then feasible to assume that the transient solution, which describes the evolution from the zero underpressure to the infinite underpressure limit, also belongs to the same curve in the (γ_m, $\Pi_m(0)$, $\Omega_m(0)$) space[6] when $\mathcal{K}_m \gtrsim 1.31$. However, tempting it is to draw a conclusion of a universal curve which lumps zero, infinite, and transient underpressure solutions in the (γ_m, $\Pi_m(0)$, $\Omega_m(0)$) space in complete toughness range, this universality cannot be supported for values of toughness below above threshold value. The calculations of the transient solution for the lower range of toughness shows the lack of such universality (Lecampion and Detournay, submitted for publication).

Finally, it is of some interest to estimate physical tip underpressure range or propagation time range in which zero tip underpressure solution is a reasonable approximation for a representative set of problem parameters. For small dimensionless tip underpressure parameter $\mathcal{T}_m = (-p_t/E')(E't/\mu')^{1/3}$, the departure

[6] Projections of which onto ($\Pi_m(0)$, γ_m) and ($\Pi_m(0)$, $\Omega_m(0)$) planes are shown in Fig. 8(a) and (b), respectively.

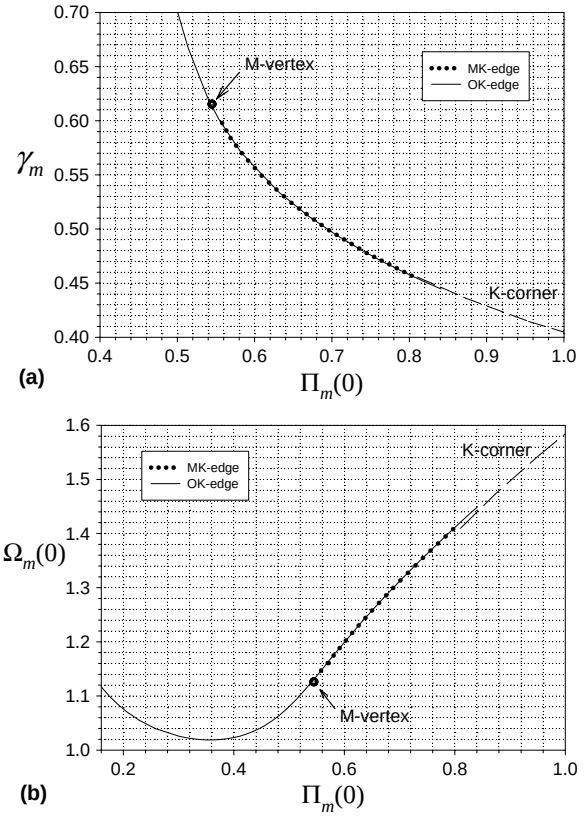

Fig. 8. Self-similar zero tip underpressure solution: the dimensionless fracture length γ_m, (a), and the dimensionless crack opening $\Omega_m(0)$ at the inlet, (b), vs. the dimensionless net-pressure at the inlet $\Pi_m(0)$. See also Fig. 7 for additional notation.

of the dimensionless transient solution from the OK-edge is $O(\mathscr{T}_m)$. By selecting 1% departure threshold ($\mathscr{T}_m = 0.01$), corresponding physical time range becomes

$$t \leqslant 10^{-6} \cdot \frac{\mu' E'^2}{(-p_t)^3} \tag{64}$$

Considering plane-strain modulus $E' = 30$ GPa representative of competent rocks and effective fracturing fluid viscosity $\mu' = 12\mu = 1$ Pa s representative of fluids used in hydraulic fracturing treatments of hydrocarbon reservoirs, above time range becomes $t \leqslant 1$ ms for $(-p_t) = 1$ MPa and $t \leqslant 10^3$ s for $(-p_t) = 10$ KPa. The 1 ms time range for the tip underpressure of 1 MPa corresponds to very short fractures for which the details of the fracture source region (e.g., finiteness of the pressurized borehole) not accounted for in this analysis, may drastically alter the solution. Nevertheless, the zero underpressure solution, even if not physically observable in this case, would provide an appropriate initial condition for numerical computations of the transient lag solution applicable at the later stages of crack propagation. On the other hand, for low values of the tip underpressure (e.g., 10 KPa), the zero underpressure solution can adequately describe hydraulic fracture propagation in physically meaningful time range. Low values of tip underpressure $(-p_t) = \sigma_o - p_{f(tip)}$ can occur either in the near-free-surface fracture when both the absolute underpressure σ_o and the pressure in the lag $p_{f(tip)}$ (bounded from above by the ambient reservoir pore pressure) are small, or in the deep fracture in the "overpressured" permeable reservoirs when $p_{f(tip)}$ is related to the ambient pore pressure which is approaching the least principle stress (Economides and Nolte, 2000).

Geophysical problem of an ascending magma dyke near the Earth's surface or of a laterally-propagating magma-filled fractures (sills) from a near-surface magma chamber are another examples where a possible low tip underpressure and large magma viscosity would promote fluid lagging. Indeed, the exsolved volatiles pressure $p_{f(tip)}$ in the tip cavity can be relatively high and comparable to confining stress σ_o levels at depths

between several hundred meters to a kilometer (Lister and Kerr, 1991). Thus, low values of the tip underpressure in the above depth range and high magma viscosity[7] may render the zero underpressure solution relevant in an extended time range of propagation (64). Consequently, fluid lag can have a direct effect on the dyke interaction with and the breakthrough through the Earth's surface and on the magma lateral emplacement. The modeling of these phenomena, however, requires additional considerations for the fluid buoyancy effect (Lister, 1990) and/or for the free surface (crack in elastic half-space).

6. Conclusions

The problem of a plane-strain fluid-driven fracture with a fluid lag in an elastic medium has been addressed under the condition of zero fluid leak-off. Through investigation of scaling, the set of problem parameters has been reduced to the two lumped dimensionless parameters: a constant $\mathscr{K}_m = K'/(E'^{3/4}Q_o^{1/4}\mu'^{1/4})$ with the meaning of dimensionless toughness and a time-varying $\mathscr{T}_m = (-p_t/E')(E't/\mu')^{1/3}$ parameter with the meaning of dimensionless underpressure in the lag region. The former uniquely defines solution trajectory in the problem parametric space while the latter prescribes evolution along the trajectory. This evolution takes place between the two limiting solutions corresponding to the zero and infinite values of the tip underpressure/time parameter $\mathscr{T}_m$ and is accompanied by the decreasing fluid lag from the maximum value (as a fraction of fracture length) at $\mathscr{T}_m = 0$ to the zero at $\mathscr{T}_m = \infty$. Similarly to the infinite tip underpressure, zero-lag solution of Spence and Sharp (1985), the zero tip underpressure solution is self-similar; i.e., when expressed in terms of the similarity variable $\xi = x/\ell(t)$, it depends on time through the scaling factors only. The zero tip underpressure solution for the fracture half-length, fluid fraction, fluid net-pressure, and crack opening has the following form, respectively:

$$\begin{aligned}
\ell(t) &= \frac{E'^{1/6}Q_o^{1/2}t^{2/3}}{\mu'^{1/6}}\gamma_m(\mathscr{K}_m)\\
\ell_f(t)/\ell(t) &= \xi_f(\mathscr{K}_m)\\
p_f(x,t) - \sigma_o &= \frac{\mu'^{1/3}E'^{2/3}}{t^{1/3}}\Pi_m(\xi;\mathscr{K}_m)\\
w(x,t) &= \frac{\mu'^{1/6}Q_o^{1/2}t^{1/3}}{E'^{1/6}}\Omega_m(\xi;\mathscr{K}_m)
\end{aligned} \tag{65}$$

This new solution provides the insight into the fracture propagation at early time or in the low tip underpressure environment. Notably, the fluid lag has a profound effect on the solution in the lower range of dimensionless toughness. The new analytical solution in the small toughness, small underpressure/time limit (the O-corner solution) shows that injected fluid is localized to an inlet boundary layer and the most of fracture length is accommodated by the lag. Corresponding crack shape away from the inlet is given by that of a crack loaded by a pair of point forces at the inlet. On the other hand, the fluid lag is exponentially small for large enough dimensionless toughness, and the zero, the transient, and the infinite underpressure solutions collapse onto the same asymptotic large-toughness solution, the K-corner solution, (Garagash, in press).

The new solutions developed in this work are relevant to the problem of a fluid-driven fracture propagation in the low underpressure environment or at early stages of the propagation. Interesting extensions of this work motivated by both engineering and geophysical applications would include the study of (i) the interaction between the fluid lag and the free surface for a near-free-surface hydraulic fractures and magma dykes; and (ii) the flow of the pore fluid between the permeable saturated solid and the fracture tip cavity (lag).

Acknowledgment

Acknowledgment is made to the Donors of The Petroleum Research Fund, administered by the American Chemical Society, for partial support of this research under Grant ACS-PRF 36729-G2.

[7] E.g, μ' can be of the order of 10^2 to 10^3 Pa s for basalts and 10^6 to 10^9 Pa s for rhyolites.

Appendix A. Normalized equations in terms of the crack coordinate ξ

Introducing scaling, Eqs. (12)–(15), into governing equations (3)–(11) we can obtain the set of equations governing the solution for the dimensionless opening, pressure, crack length, and fluid fraction, $\mathscr{F}(\xi,t)=\{\Omega,\Pi,\gamma,\xi_f\}$ expressed in terms of the crack coordinate $\xi=\xi_f\zeta$ and time. (Alternative system of normalized equations in terms of the channel coordinate ζ is presented in the main text, Eqs. (17)–(22).) Using the rescaled opening $\bar{\Omega}=\Omega/\gamma$, Eq. (16), these equations are as follows.

- Lubrication equation, $\xi\in(0,\xi_f)$

$$\left[1+2\frac{t\dot{\gamma}}{\gamma}\right]\int_\xi^{\xi_f}\bar{\Omega}\,d\xi+\left[\delta+\frac{t\dot{\gamma}}{\gamma}\right]\xi\bar{\Omega}+t\dot{\xi}_f\bar{\Omega}_{|\xi=\xi_f}+\int_\xi^{\xi_f}t\dot{\bar{\Omega}}\,d\xi=-\frac{\bar{\Omega}^3}{\mathscr{M}}\frac{\partial\Pi}{\partial\xi} \tag{A.1}$$

  The overdot in Eq. (A.1) corresponds to the time derivative at fixed ξ, $\frac{\partial}{\partial t|_\xi}=\frac{\partial}{\partial t|_\zeta}-\frac{\dot{\xi}_f}{\xi_f}\zeta\frac{\partial}{\partial\zeta}$, and $\delta=t\dot{L}/L$ is equal to a constant 2/3 for fracture scalings defined in Section 3.2.
- Pressure condition in the lag

$$\Pi=-\mathscr{T},\quad \xi\in[\xi_f,1] \tag{A.2}$$

- Global continuity

$$2\gamma^2\int_0^{\xi_f}\bar{\Omega}\,d\xi=1 \tag{A.3}$$

- Elasticity

$$\bar{\Omega}=\int_0^{\xi_f}G(\xi,\xi')\Pi(\xi',t)\,d\xi'-\mathscr{T}\int_{\xi_f}^1G(\xi,\xi')\,d\xi',\quad \xi\in(0,1) \tag{A.4}$$

- Propagation condition

$$\bar{\Omega}=\mathscr{K}\gamma^{-1/2}(1-\xi)^{1/2},\quad 1-\xi\ll 1 \tag{A.5}$$

  or, alternatively,

$$\mathscr{K}=\frac{2^{7/2}}{\pi}\gamma^{1/2}\left(\int_0^{\xi_f}\frac{\Pi\,d\xi}{\sqrt{1-\xi^2}}-\mathscr{T}\arccos\xi_f\right) \tag{A.6}$$

  Table 1 provides expressions of governing dimensionless groups $\mathscr{M}$, $\mathscr{K}$, and $\mathscr{T}$ in the viscosity and toughness scalings.

Appendix B. Numerical scheme for zero underpressure/time solution (OK-edge)

To obtain numerical solution for intermediate values of $\mathscr{K}_m$, $0<\mathscr{K}_m<\infty$, we will use the methodology similar to the one suggested by Garagash and Detournay (2000) for the solution of a semi-infinite hydraulic fracture with a lag. The fluid channel $0\leqslant\xi\leqslant\xi_f(\mathscr{K}_m)$ is an unknown function of $\mathscr{K}_m$ which is a part of the solution. Instead of solving the problem equations in unknown domain, we prescribe the fluid domain, i.e. the fluid fraction ξ_f, and then obtain toughness parameter $\mathscr{K}_m$ as a part of the numerical solution $\{\Pi_m(\xi;\xi_f),\Omega_m(\xi;\xi_f),\gamma_m(\xi_f),\mathscr{K}_m(\xi_f)\}$. The numerical procedure described below consist of the two main steps. First, we use a piecewise linear approximation of the net-pressure over the fluid channel in the elasticity equation to find corresponding closed-form expression for the crack opening. Secondly, these approximations for the pressure and opening are used to form a finite difference approximation of the lubrication equation, which together with the zero net-pressure boundary condition at the fluid front and the propagation criterion constitute a non-linear system of algebraic equations on the unknown values of the net-pressure Π at the grid points along the channel and toughness $\mathscr{K}_m$. This set of equations is solved using the *Newton* iteration procedure in the Mathematica software, version 4.1 (© 1988–2001 Wolfram Research, Inc.).

We start by introducing the set of $N+1$ grid points $\{\xi_i\}$, $i=1,\ldots,N+1$, with $\xi_1=0$ and $\xi_{N+1}=\xi_f$, and approximating pressure $\Pi_m(\xi)$ as a piecewise linear function over a set of grid intervals $[\xi_i, \xi_{i+1}]$, such that

$$\Pi_m(\xi) = a_i + b_i\xi, \quad \xi \in [\xi_i, \xi_{i+1}], \;\; i=1,\ldots,N \tag{B.1}$$

Using the pressure continuity at a grid point, the a's and b's are expressed in terms of the unknown values of the pressure at the grid points, $\Pi_{(i)} = \Pi_m(\xi_i)$, as

$$a_i = \Pi_{(i)} - \xi_i \frac{\Pi_{(i+1)} - \Pi_{(i)}}{\xi_{i+1} - \xi_i}, \quad b_i = \frac{\Pi_{(i+1)} - \Pi_{(i)}}{\xi_{i+1} - \xi_i} \tag{B.2}$$

Substitution of Eq. (B.1) in the elasticity equation (61) yields an explicit expression for the fracture opening

$$\bar{\Omega}_m(\xi) = \sum_{i=1}^{N} \left[a_i I_1(\xi,\xi') + b_i I_2(\xi,\xi')\right]_{\xi'=\xi_i}^{\xi'=\xi_{i+1}} \tag{B.3}$$

Functions I_1 and I_2 can be found in the form

$$\begin{aligned} I_1(\xi,\xi') &= \int G(\xi,\xi')\,\mathrm{d}\xi' \\ &= \frac{8}{\pi}\sqrt{1-\xi^2}\arcsin\xi' + \xi' G(\xi,\xi') + \xi\left(\frac{4}{\pi}\ln\left|\frac{\xi-\xi'}{\xi+\xi'}\right| + F_+(\xi,\xi')\right) \\ I_2(\xi,\xi') &= \int \xi' G(\xi,\xi')\,\mathrm{d}\xi' = \frac{1}{2}(\xi'^2-\xi^2)G(\xi,\xi') - \frac{4}{\pi}\sqrt{1-\xi'^2}\sqrt{1-\xi^2} \end{aligned}$$

where complimentary functions $F_\pm$ are defined as

$$F_\pm(\xi,\xi') = \frac{4}{\pi}\ln\frac{1+\xi'\xi \pm \sqrt{1-\xi'^2}\sqrt{1-\xi^2}}{1-\xi'\xi \pm \sqrt{1-\xi'^2}\sqrt{1-\xi^2}}$$

Let us designate the left and the right hand sides of the lubrication equation $(59)_a$ by $\Phi_m(\xi)$ and $\Psi_m(\xi)$, respectively. Then, $\Psi_m(\xi)$ is easily evaluated from Eqs. (B.1) and (B.3)

$$\Psi_m(\xi) = -b_i\bar{\Omega}_m^3(\xi), \quad \xi \in [\xi_i, \xi_{i+1}], \;\; i=1,\ldots,N \tag{B.4}$$

Using Eq. (B.3), $\Phi_m(\xi)$ can be evaluated in the following form:

$$\Phi_m(\xi) = \sum_{i=1}^{N}\left[a_i\left(J_1(\xi_f,\xi') - J_1(\xi,\xi') + \frac{2}{3}\xi I_1(\xi,\xi')\right) + b_i\left(J_2(\xi_f,\xi') - J_2(\xi,\xi') + \frac{2}{3}\xi I_2(\xi,\xi')\right)\right]_{\xi'=\xi_i}^{\xi'=\xi_{i+1}} \tag{B.5}$$

Functions J_1 and J_2 are given by

$$\begin{aligned} J_1(\xi,\xi') &= \int I_1(\xi,\xi')\,\mathrm{d}\xi = \frac{1}{2}\xi'^2 F_-(\xi,\xi') + \frac{1}{2}(2\xi'^2+\xi^2)F_+(\xi,\xi') + \xi'\xi G(\xi,\xi') \\ &\quad + \frac{4}{\pi}\left(\xi'\sqrt{1-\xi'^2}\arcsin\xi + \arcsin\xi'\left(\xi\sqrt{1-\xi^2} + \arcsin\xi\right) + \frac{1}{2}(3\xi'^2+\xi^2)\ln\left|\frac{\xi-\xi'}{\xi+\xi'}\right|\right) \\ J_2(\xi,\xi') &= \int I_2(\xi,\xi')\,\mathrm{d}\xi = \frac{1}{6}\xi'^2(\xi' F_-(\xi,\xi') + 3\xi' F_+(\xi',\xi) + 3\xi G(\xi',\xi)) \\ &\quad + \frac{4}{3\pi}\left(-\xi\sqrt{1-\xi'^2}\sqrt{1-\xi^2} - 2(1-\xi'^2)^{3/2}\arcsin\xi\right) - \frac{1}{6}\xi^3 G(\xi,\xi') + \frac{8}{3\pi}\xi'^3\ln\left|\frac{\xi-\xi'}{\xi+\xi'}\right| \end{aligned}$$

In the view of expressions for a's and b's, Eq. (B.2), and the pressure boundary condition at the fluid front, $\Pi_{(N+1)}=0$, the set of N non-linear algebraic equations corresponding to the lubrication equation evaluated at the mid-points of grid intervals

$$\Phi_m(\xi_{i+1/2}) = \Psi_m(\xi_{i+1/2}), \quad \xi_{i+1/2} = \frac{\xi_i + \xi_{i+1}}{2}, \ \ i = 1, \ldots, N \tag{B.6}$$

is solved for the N unknown values of pressure at the grid points: $\Pi_{(1)}, \Pi_{(2)}, \ldots, \Pi_{(N)}$.

Upon attaining solution for $\Pi_m(\xi)$, Eq. (B.1) with Eq. (B.2), and $\bar{\Omega}_m(\xi)$, Eq. (B.3), corresponding to the specified position of the fluid front ξ_f, the fracture dimensionless length γ_m, and corresponding value of dimensionless toughness $\mathcal{K}_m$ are computed by evaluating expressions (60) and $(62)_a$, respectively,

$$\gamma_m^{-2} = 2\sum_{i=1}^{N}[a_i J_1(\xi_f, \xi') + b_i J_2(\xi_f, \xi')]_{\xi'=\xi_i}^{\xi'=\xi_{i+1}} \tag{B.7}$$

$$\mathcal{K}_m = \frac{2^{7/2}}{\pi}\gamma_m^{1/2}\sum_{i=1}^{N}\left[a_i \arcsin\xi - b_i\sqrt{1-\xi^2}\right]_{\xi=\xi_i}^{\xi=\xi_{i+1}} \tag{B.8}$$

Large toughness, small lag calculations. As toughness $\mathcal{K}_m$ increases to large values or, equivalently, fluid lag $1-\xi_f$ decreases in the zero underpressure/time solution, the net-pressure gradient near the fluid front becomes large. This can be seen from the leading term of the near tip asymptote of the net-pressure resulting from using the near tip opening asymptote $(62)_b$ in the lubrication equation (59) under condition that $1-\xi_f \ll 1-\xi \ll 1$, $\Pi_m = (2\gamma_m/3\mathcal{K}_m^2)\ln(1-\xi^2)$. Note also that the latter asymptote is equivalent to the large-toughness asymptote (53) in the view of the K-vertex solution (48) and scaling relations (26), (27).

The solution scheme based on the piecewise linear pressure approximation on a uniform grid along the fluid channel, Eq. (B.1), is not suited to capture large pressure gradient near the fluid front at large toughness. To improve the scheme and its accuracy in this limit, we express the net-pressure as the sum of logarithmic ('tip') and regular terms

$$\Pi_m(\xi) = \Pi_{m(\mathrm{tip})}(\xi) + \Pi_{m(\mathrm{reg})}(\xi) \tag{B.9}$$

where $\Pi_{m(\mathrm{tip})}$ is taken in the form

$$\Pi_{m(\mathrm{tip})}(\xi) = \frac{2\gamma_m}{3\mathcal{K}_m^2}\xi\ln(1-\xi^2) \tag{B.10}$$

asymptotically equivalent to the one discussed above. (The latter has been multiplied by ξ to arrive to Eq. (B.10) in order to simplify integration of elasticity equation (61).) For the regular part of the net-pressure we adopt a piecewise linear approximation, as previously in Eq. (B.1),

$$\Pi_{m(\mathrm{reg})}(\xi) = a_i + b_i\xi, \quad \xi \in [\xi_i, \xi_{i+1}], \ \ i = 1, \ldots, N \tag{B.11}$$

Continuity of $\Pi_{m(\mathrm{reg})}$ at a grid point yields expressions (B.2) for a's and b's where now $\Pi_{(i)} = \Pi_{m(\mathrm{reg})}(\xi_i)$, $i = 1, \ldots, N+1$.

Expression for the fracture opening, Eq. (B.3), is modified accordingly

$$\bar{\Omega}_m(\xi) = \bar{\Omega}_{m(\mathrm{tip})}(\xi) + \sum_{i=1}^{N}[a_i I_1(\xi, \xi') + b_i I_2(\xi, \xi')]_{\xi'=\xi_i}^{\xi'=\xi_{i+1}} \tag{B.12}$$

with

$$\bar{\Omega}_{m(\mathrm{tip})}(\xi) = \int_0^{\xi_f} G(\xi, \xi')\Pi_{m(\mathrm{tip})}(\xi')\,\mathrm{d}\xi' = \frac{2\gamma_m}{3\mathcal{K}_m^2}\left[-\frac{2}{\pi}F_{\ln}(1-\xi^2, 1-\xi'^2)\right]_{\xi'=0}^{\xi'=\xi_f}$$

In the above expression, function $F_{\ln}$ is defined by

$$F_{\ln}(z, z') = \int \ln\left|\frac{z^{1/2}+z'^{1/2}}{z^{1/2}-z'^{1/2}}\right| \ln z'\,\mathrm{d}z' = 2(zz')^{1/2}(\ln z' - 3) + (z-z')(1-\ln z')\ln\left|\frac{z^{1/2}+z'^{1/2}}{z^{1/2}-z'^{1/2}}\right| + 2z f_{\ln}(z'/z)$$

where complimentary function $f_{\ln}$ is given by

$$f_{\ln}(z)=\begin{cases}\mathrm{Li}_2(z^{1/2})-\mathrm{Li}_2(-z^{1/2}), & z<1,\\ \pi^2/4, & z=1,\\ \mathrm{Li}_2(-z^{-1/2})-\mathrm{Li}_2(z^{-1/2})+\pi^2/2, & z>1,\end{cases}$$

The discretized form (B.6) of the lubrication equation $(59)_a$ is then updated to include the contributions from the 'tip' term $\bar{\Omega}_{m(\mathrm{tip})}$. Similarly, the right hand sides of expression (B.7) of the global balance equation (60), and of expression (B.8) of the propagation condition $(62)_a$ are updated to include the respective 'tip' contributions $2\int_0^{\xi_f}\bar{\Omega}_{m(\mathrm{tip})}\,\mathrm{d}\xi$ and $\mathscr{K}_{m(\mathrm{tip})}=\frac{8}{\pi}\frac{(2\gamma_m)^{3/2}}{3\mathscr{K}_m'^2}\left[-2+\sqrt{1-\xi_f^2}(2-\ln(1-\xi_f^2))\right]$. The updated form of non-linear equations (B.6)–(B.8) together with the zero net-pressure condition at the fluid front is solved for γ_m, $\mathscr{K}_m$, and N values of $\Pi_{m(\mathrm{reg})}$ at the grid points: $\Pi_{(1)}, \Pi_{(2)}, \ldots, \Pi_{(N)}$.

References

Abé, H., Mura, T., Keer, L.M., 1976. Growth rate of a penny-shaped crack in hydraulic fracturing of rocks. J. Geophys. Res. 81, 5335–5340.

Adachi, J.I., 2001. Fluid-driven fracture in permeable rock. Ph.D. Thesis, University of Minnesota.

Adachi, J.I., Detournay, E., 2002. Self-similar solution of a plane-strain fracture driven by a power-law fluid. Int. J. Numer. Anal. Methods Geomech. 26, 579–604.

Advani, S., Lee, T., Dean, R., Pak, C., Avasthi, J., 1997. Consequences of fluid lag in three-dimensional hydraulic fractures. Int. J. Numer. Anal. Methods Geomech. 21, 229–240.

Au, S., 2001. Fundamental study of compensation grouting. Ph.D. Thesis, University of Cambridge.

Barenblatt, G.I., 1956. On the formation of horizontal cracks in hydraulic fracture of an oil-bearing stratum. Prikl. Mat. Mech. 20, 475–486.

Batchelor, G.K., 1967. An Introduction to Fluid Dynamics. Cambridge University Press, Cambridge, UK.

Bilby, B., Eshelby, J., 1968. Dislocations and the theory of fracture. In: Liebowitz, H. (Ed.), Fracture, an Advanced Treatise, vol. I. Academic Press, New York, NY, pp. 99–182 (Chapter 2).

Bui, H.D., 1996. Interaction between the Griffith crack and fluid: theory of Rehbinder's effect. In: Cherepanov, G.P. (Ed.), Fracture: A Topical Encyclopedia of Current Knowledge. Krieger.

Bunger, A.P., Detournay, E., Jeffrey, R.G., 2005. Crack tip behavior in near-surface fluid-driven fracture experiments. C. R. Acad. Sci. Paris 333, 299–304.

Carbonell, R., Desroches, J., Detournay, E., 1999. A comparison between a semi-analytical and a numerical solution of a two-dimensional hydraulic fracture. Int. J. Solids Structures 36 (31–32), 4869–4888.

Desroches, J., Detournay, E., Lenoach, B., Papanastasiou, P., Pearson, J.R.A., Thiercelin, M., Cheng, A.H.-D., 1994. The crack tip region in hydraulic fracturing. Proc. Roy. Soc. Lond., Ser. A (447), 39–48.

Detournay, E., 1999. Fluid and solid singularities at the tip of a fluid-driven fracture. In: Durban, D., Pearson, J. (Eds.), Proceedings of the IUTAM Symposium on Non-Linear Singularities in Deformation and Flow, Haifa. Kluwer Academic Publishers, Dordrecht, pp. 27–42.

Detournay, E., 2004. Propagation regimes of fluid-driven fractures in impermeable rocks. Int. J. Geomech. 4 (1), 1–11.

Detournay, E., Garagash, D., 2003. The tip region of a fluid-driven fracture in a permeable elastic solid. J. Fluid Mech. 494, 1–32.

Economides, M.J., Nolte, K.G. (Eds.), 2000. Reservoir Stimulation, third ed. John Wiley & Sons, Chichester, UK.

Garagash, D.I., 2000. Hydraulic fracture propagation in elastic rock with large toughness. In: Girard, J., Liebman, M., Breeds, C., Doe, T. (Eds.), Pacific Rocks 2000—Proceedings of the 4th North American Rock Mechanics Symposium. Balkema, Rotterdam, pp. 221–228.

Garagash, D.I., in press. Plane strain propagation of a hydraulic fracture during injection and shut-in: asymptotics of large toughness. Eng. Frac. Mech, doi:10.1016/j.engfracmech.2005.07.012.

Garagash, D.I., Detournay, E., 2000. The tip region of a fluid-driven fracture in an elastic medium. ASME J. Appl. Mech. 67 (1), 183–192.

Garagash, D.I., Detournay, E., 2002. Viscosity-dominated regime of a fluid-driven fracture in an elastic medium. In: IUTAM Symposium on Analytical and Computational Fracture Mechanics of Non-Homogeneous Materials, Cardiff. In: Karihaloo, B.L. (Ed.), Solid Mechanics and its Applications, vol. 97. Kluwer Academic Publishers, Dordrecht, pp. 25–29.

Garagash, D.I., Detournay, E., 2005. Plane-strain propagation of a fluid-driven fracture: small toughness solution. ASME J. Appl. Mech. 72 (6), 916–928.

Geertsma, J., de Klerk, F., 1969. A rapid method of predicting width and extent of hydraulic induced fractures. J. Pet. Tech. 246, 1571–1581 (SPE 2458).

Groenenboom, J., van Dam, D.B., de Pater, C.J., 2001. Time-lapse ultrasonic measurements of laboratory hydraulic-fracture growth: tip behavior and width profile. Soc. Pet. Eng. J. 6 (1), 14–24.

Huang, N., Szewczyk, A., Li, Y., 1990. Self-similar solution in problems of hydraulic fracturing. ASME J. Appl. Mech. 57, 877–881.

Irvin, G.R., 1957. Analysis of stresses and strains near the end of a crack traversing a plate. ASME J. Appl. Mech. 24, 361–364.

Jeffrey, R.G., 1989. The combined effect of fluid lag and fracture toughness on hydraulic fracture propagation. In: Joint Rocky Mountain Regional/Low Permeability Reservoirs Symposium and Exhibition, March 6–8. Society of Petroleum Engineers, Denver, CO, pp. 269–276.

Jeffrey, R.G., Mills, K.W., 2000. Hydraulic fracturing applied to inducing longwall coal mine goaf falls. In: Girard, J., Liebman, M., Breeds, C., Doe, T. (Eds.), Pacific Rocks 2000—Proceedings of the 4th North American Rock Mechanics Symposium. Balkema, Rotterdam, pp. 423–430.

Kanninen, M.F., Popelar, C.H., 1985. Advanced Fracture Mechanics. The Oxford Engineering Science Series, vol. 15. Oxford University Press, Oxford UK.

Khristianovic, S., Zheltov, Y., 1955. Formation of vertical fractures by means of highly viscous fluids. In: Proceedings of the 4th World Petroleum Congress, Rome, vol. II, pp. 579–586.

Lecampion, B., Detournay, E., submitted for publication. An implicit algorithm for the propagation of a hydraulic fracture with a lag. Comput. Methods Appl. Mech. Eng.

Lister, J.R., 1990. Buoyancy-driven fluid fracture: the effects of material toughness and of low-viscosity precursors. J. Fluid Mech. 210, 263–280.

Lister, J.R., Kerr, R.C., 1991. Fluid-mechanical models of crack propagation and their applications to magma transport in dykes. J. Geophys. Res. 96 (B6), 10,049–10,077.

Medlin, W., Masse, L., 1984. Laboratory experiments in fracture propagation. Soc. Pet. Eng. J. (June), 256–268.

Murdoch, L.C., 2002. Mechanical analysis of idealized shallow hydraulic fracture. J. Geotech. Geoenviron. Eng. 128 (6), 488–495.

Nilson, R., 1981. Gas driven fracture propagation. ASME J. Appl. Mech. 48, 757–762.

Perkins, T.K., Kern, L.R., 1961. Widths of hydraulic fractures. J. Pet. Tech., Trans. AIME 222, 937–949.

Rubin, A.M., 1993. Tensile fracture of rock at high confining pressure: implications for dike propagation. J. Geophys. Res. 98 (B9), 15,919–15,935.

Rudnicki, J.W., 2000. Geomechanics. Int. J. Solids Structures 37, 349–358, also appeared as a chapter in the volume Research Trends in Solid Mechanics, Report from the US National Committee on Theoretical and Applied Mechanics, editor George J. Dvorak, Elsevier, 1999.

Savitski, A., Detournay, E., 2002. Propagation of a fluid-driven penny-shaped fracture in an impermeable rock: asymptotic solutions. Int. J. Solids Structures 39 (26), 6311–6337.

Sneddon, I., Lowengrub, M., 1969. Crack Problems in the Classical Theory of Elasticity. John Wiley & Sons, New York, NY.

Spence, D., Turcotte, D., 1985. Magma-driven propagation of cracks. J. Geophys. Res. 90, 575–580.

Spence, D.A., Sharp, P.W., 1985. Self-similar solution for elastohydrodynamic cavity flow. Proc. Roy. Soc. Lond., Ser. A (400), 289–313.